



**2020 AASE
INTERNATIONAL
CONFERENCE**

**BESM-43
ETAS-42**

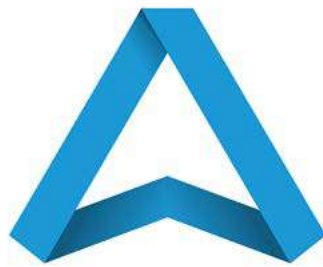
- *43th International Conference on Business, Education, Social Science, and Management*
- *42th International Conference on Engineering, Technology and Applied Science*

JAN · 14-15 · 2020 @ TOKYO/JAPAN





**PROCEEDINGS OF
AASE INTERNATIONAL CONFERENCE
42th ETAS & 43th BESM Conference**



Applied and Advanced Science Exchange (AASE)

Published by



Warning: No part of this book can be reproduced in any form or by any means without prior written permission of the publisher.

© 2020, The AASE International Conference

International Conference on Engineering, Technology and Applied Science (ETAS)

- 42th ETAS @ Tokyo/Japan, Jan.14th-15th, 2020

International Conference on Business, Education, Social Science, and Management (BESM)

- 43th BESM @ Tokyo/Japan, Jan.14th-15th, 2020

Publication title: PROCEEDINGS OF AASE INTERNATIONAL CONFERENCE 42th ETAS & 43th BESM
Conference

Edited by: Applied and Advanced Science Exchange (AASE)

Publisher: Association of Advanced Science Exchange

Telephone: +886-905-463-331

<https://www.aaseconference.org/>

ISBN Code:

ISBN 978-986-97484-4-5



9 789869 748445

Applied and Advanced Science Exchange (AASE):

The *Applied and Advanced Science Exchange* (AASE) is an active professional community and registered as a non-profit organization (NGO) in Japan. AASE has devoted itself to disseminate a variety of knowledge and worked with a vision to share the innovations in fields of academia by building up an international platform. Nowadays, interdisciplinary research is increasing and playing a key role. In our interdisciplinary joint conferences, participants are able to share their viewpoints from different perspectives and seek new collaborative opportunities across fields.

The *Applied and Advanced Science Exchange* (AASE) offers an extraordinary platform for networking opportunities and discussions to enhance research progress in various fields. From 2016, we have run a series of professional workshops, conferences, seminars and symposiums, and have built a reputation for delivering inspirational conferences with flawless execution. Our purpose is to facilitate networking opportunities for scholars and be the information resources for dynamic professional development opportunities throughout the World.



AASE conferences footprints of the world

EDITORIAL MESSAGE

It is my proud privilege to welcome you all to the AASE International Conference at Seoul/South Korea on 14th-15th Jan, 2020. AASE International Conference serves as platform that aims to provide opportunity to the academicians and scholars from across various disciplines to discuss interdisciplinary innovations. We are happy to see the papers from all part of the world published in this proceedings. This proceeding brings out the various Research papers from diverse areas of science, engineering, technology, management, business and education. These articles that we received for these conferences are very promising and impactful. We believe these studies have the potential to address key challenges in various sub-domains of social sciences and applied sciences. I am really thankful to all the participants for being here with us to create an environment of knowledge sharing and learning. I am also thankful to our scientific and review committee for spending much of their time in reviewing the papers for these events. I am sure the contributions by the authors shall add value to the research community.

Editor-In-Chief
Dr. H. Miyamoto

TABLE OF CONTENTS

No	TITLES/AUTHORS	Page No.
	COPY RIGHT PAGE	ii
	APPLIED AND ADVANCED SCIENCE EXCHANGE (AASE)	iii
	EDITORIAL MESSAGE	iv
01.	Landslide Risk Perception of On-road Residents along Sino-Nepal Transportation Corridor ➤ <i>Susmita Dhakal</i>	1-2
02.	When morphology instruction meets learning strategies in lexical acquisition, effective or complex? ➤ <i>Sheng- Huang Huang</i>	3
03.	Compression-shear Behavior of Rubber Sealed Joints ➤ <i>Waranyoo Prombandankul</i>	4-10
04.	PAPIdroid : A Risk Scoring of Android Malware Apps Based on Permissions and API Call ➤ <i>Mardiyansyah</i>	11-23
05.	Development of Travel Demand Models under Earthquake by Using Spaghetti and Meatballs Method and Four-Step Transportation Model ➤ <i>Jessada Pochan</i>	24-35
06.	Piano Keyboard 3D Pedestrian Crossing Evaluation: The case of Chiang Mai University Demonstration School ➤ <i>Preda Pichayapan</i>	36-45

Landslide Risk Perception of On-road Residents along Sino-Nepal Transportation Corridor

Susmita Dhakal^{ab}, Peng Cui^{1*}, Li-jun Su^a, Chandra Prasad Rijal^c, Ashok Maharjan^b

^aInstitute of Mountain Hazard and Environment, Chinese Academy of Science, China

^bCentral Department of Environmental Science, Tribhuvan University, Nepal

^cTourism Search and Rescue Guidance Committee, Government of Nepal

*Corresponding author: pengcui@imde.ac.cn

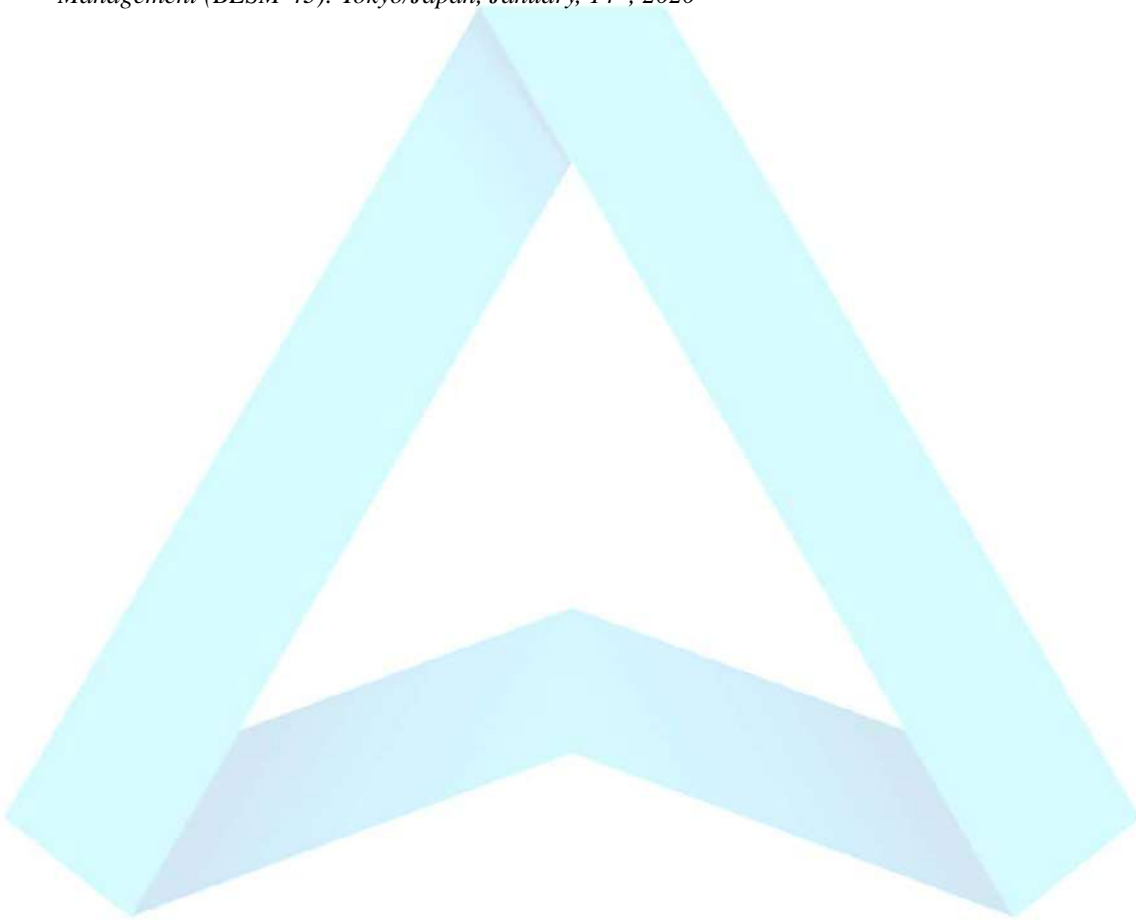
Abstract

Landslide, a frequent hazard along Sino-Nepal transportation corridor is the result of interaction of tectonic movement – 1.8 to 2 cm/year, constant river incision, young and weak geology, and monsoonal weather and climate system, and development activities. Currently, the area further planned not only for the high grade highway but also for the transboundary railway. This study aims to analyze how people perceive the landslide risk in their surroundings. We applied key informant interview (40), focus group discussion (5) and questionnaire survey (296) amongst residents of 8 on-road towns. Mapping and analysis of the current state of the past road blocking events that have influenced the risk perception of populace were done using high resolution satellite images and field investigations. All respondents have memory of one or more past event(s) however, only 87% could define landslide hazard. The rated risk with the consideration of probability of landslide occurrences, its impact on human, property, business, and preparedness counting internal and external capacities varies through town to town that ranged between 13-37% (min) and 59-94% (max) with median value of 29.5 to 62%. Public understanding of landslide risk was affected by practical experiences (47%), news-media (29%), interaction with community (15%) and formal education (9%). Only 2% respondents got basic training of disaster risk. Locals have differential trust on organizations as well as their activities i.e. low (35%), medium (47%), and high (17%). Most of them have faith to the government entities, the highest to the army; non-governmental organizations are at the lowest. Elected persons of local governments and district level government officers have disbelief to the current researches whereas locals and sufferers of past events have dissatisfaction to the ongoing mitigation activities. Victims and eyewitness of any event have more fear and higher risk ratings compared to general public. Although the notion of ‘memory dilutes over time’ was realized, rain-induced former incidents especially large landslides with reactivations, and co-seismic slope failures of 2015 tremor have great effect on perceived risk. Moreover unlike other studies, age, sex, education

and occupation of respondents did not show a distinct relationship with risk ratings; personal experiences and hardships they bear played the role instead.

Keywords: Landslide risk, Sino-Nepal transportation corridor, risk perception, landslide susceptibility

- *This research presented on 43th International Conference on Business, Education, Social Science, Management (BESM-43): Tokyo/Japan, January, 14th, 2020*



When morphology instruction meets learning strategies in lexical acquisition, effective or complex?

Sheng- Huang Huang

Department of Applied Foreign Languages, National Yunlin University of Science & Technology

*Corresponding author: m10341024@gmail.yuntech.edu.tw

Abstract

Morphology instruction has been evidenced to enhance students' language learning in recent years (Bowers, Kirby, & Deacon, 2010), but most previous studies evaluate the impact of morphology instruction on learning effectiveness, without providing relevant learning strategies. Therefore, this study integrates cognitive strategies and memory strategies into lexical learning, investigating how morphology instruction, together with both cognitive strategies and memory strategies, could promote EFL learners' vocabulary performances. The pedagogical experiment was devised as a 13-week lesson plan with 14 learners, eight being at the lower-intermediate level and another eight at the intermediate level. The participants' lexical performances assessed by means of the pre- and post-tests and in-class quizzes, were found to be statistically significant in comparison with their pre-instruction performances, particularly the underachievers' performances. Their perceptions of the given instruction examined from a self-reflection questionnaire and semi-structured interviews also reveal that they have benefitted from lexical practices, and that they have learned to apply the taught strategies to memorize new words.

Keywords: morphology instruction, vocabulary learning strategies, EFL

- *This research presented on 43th International Conference on Business, Education, Social Science, Management (BESM-43): Tokyo/Japan, January, 14th, 2020*

Compression-shear Behavior of Rubber Sealed Joints

Waranyoo Prombandankul^a, Watanachai Smittakorn^{b*}

^aTechnopreneurship and Innovation management program, Graduate school, Chulalongkorn University, Bangkok 10330, Thailand

^bApplied Mechanics and Structures research unit, Department of Civil Engineering, Chulalongkorn University, Bangkok 10330, Thailand

^abenz824824@yahoo.com, ^bwatanachai.s@chula.ac.th (Corresponding author)

Abstract

For precast concrete tunnels, joints and rubber seal in joints are commonly assumed to resist no shear between tunnel segments. However, the recent study provides evidence that the rubber seal contributes significant shear resistance to joints and suggests that shear behavior of rubber seal is needed to be studied. This paper aims to affirm this claim and study the shear behavior of rubber seals. In our experiment, Natural bearing pad rubbers are used as rubber seals. The compression-shear test is conducted with the rubber seals fixed against slippery to the steel specimen. Load cells are installed for vertically and horizontally and the vertical displacement is measured. The results show that joints with rubber seals provide higher final shear stress than unsealed joints in a confinement level. This result should lead to a new understanding of rubber seals and new application of them.

Keywords: Rubber seal, Precast concrete tunnel, Compression-shear test

➤ *This research presented on 42th International Conference on Engineering, Technology and Applied Science (ETAS-42): Tokyo/Japan, January, 14th, 2020*

1. Introduction

Precast concrete construction has been widely used for many decades in various types of construction including modern high-rise buildings, houses and bridges as well as immersed tunnels. Each precast tunnel segment is placed on top of gravel layers and connected to the next segment presuming that no shear force transfers between them [1]. Figure 1 shows the laying process and cross-sectional tunnel segment. Immersion joints are therefore designed for water tightness only. Each immersion joint consists of a "Gina gasket" rubber seal as shown in Figure 2. The rubber seal is thus designed solely to prevent water leakage.

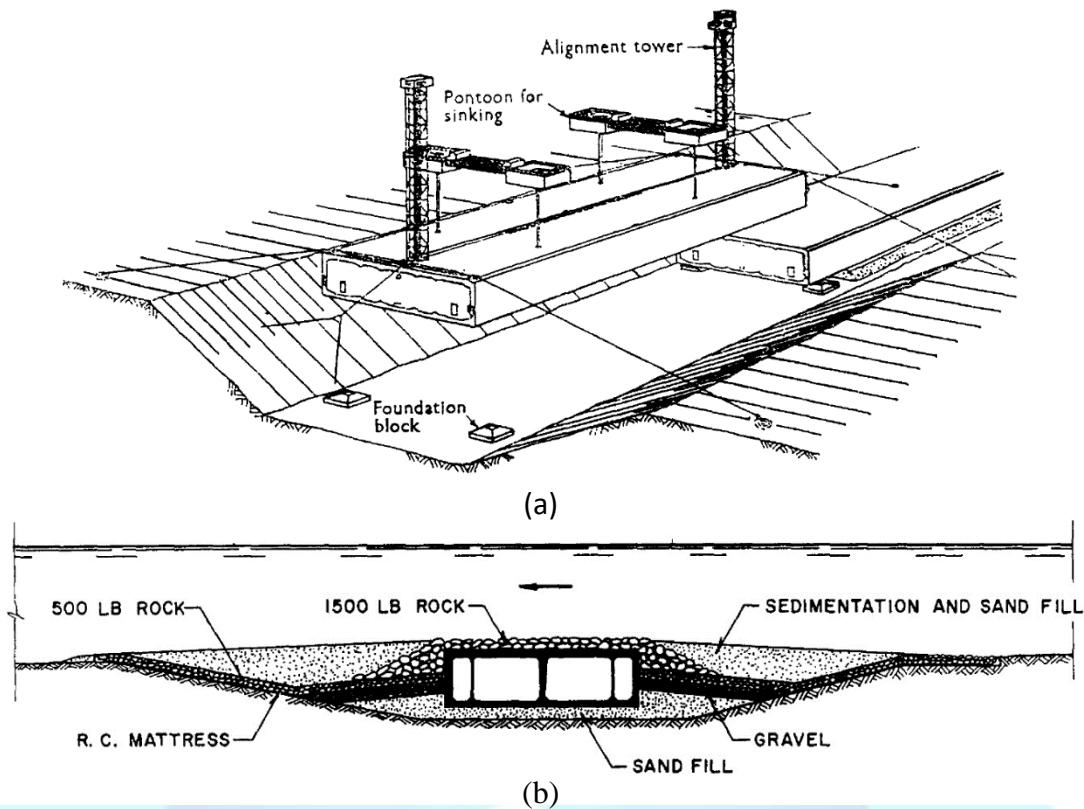


Figure 1: Precast tunnel construction [1]; (a) Laying process of tunnel segment; (b) Cross-sectional tunnel

However, when foundation settlement and earthquake are concerned, it is important to study the shear resistance of rubber in joints. The recent study provided evidence that the rubber seal gives significant shear resistance to the structure [2]. This paper therefore attempts to study the compression-shear behavior of rubber seals. Here, we choose natural rubber bearing pads to be used as rubber seals because they are capable of supporting normal stress and horizontal shear movement to structures. [3].

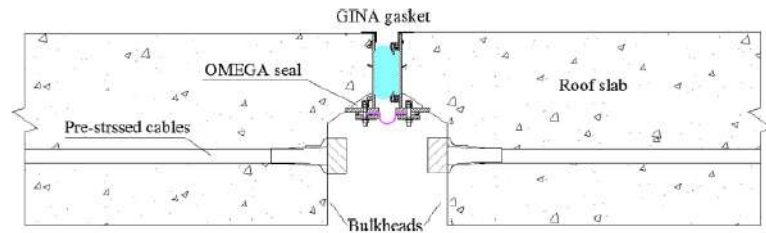
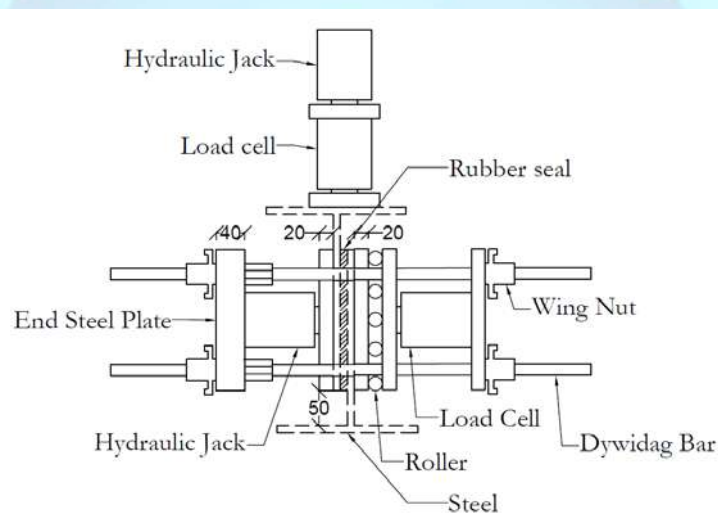


Figure 2: Detail of immersion joint and Gina gasket [4]

2. Experimental setup

This study aims to examine the ability of elastomeric bearing in joints to resist shear force. We build compression-shear experiment which allow only normal stress and shear stress without moment. As shown in figure 3(a), the specimen is T-beam steel with a height of 250 mm, a width of 200 mm and a length of 200 mm. The contact surface measures 200 mm x 200 mm. The rubber is connected to the steel beams by a 2-component thixotropic epoxy adhesive with a steel beam which prevents rubber from slipping from the metal layer. The hydraulic pump's horizontal stress simulates confinement on the rubber. Rubber seal compressive stress is 1 MPa and 2 MPa which is similar to Zhou et al. (2005) unsealed joint [5]. The load cells are installed for both axis. The LVDTs measure the vertical displacement at both side of the specimen as shown in figure 3(b). The loading rate is applied at 0.04 per second until the shear strain reaches 1. The natural bearing pad rubber is employed, according to Thai Industrial Standard 951-2533 [6], with a hardness level of 60 and 70.

The specimen descriptor is defined as Mi-HH: M denoting the corresponding monotonic load, and i reflecting axial load simulating the load of pre-stressed cables (in MPa). HH is a rubber hardness level of 60 to 70. The test is conducted up to 100% strain.



(a)

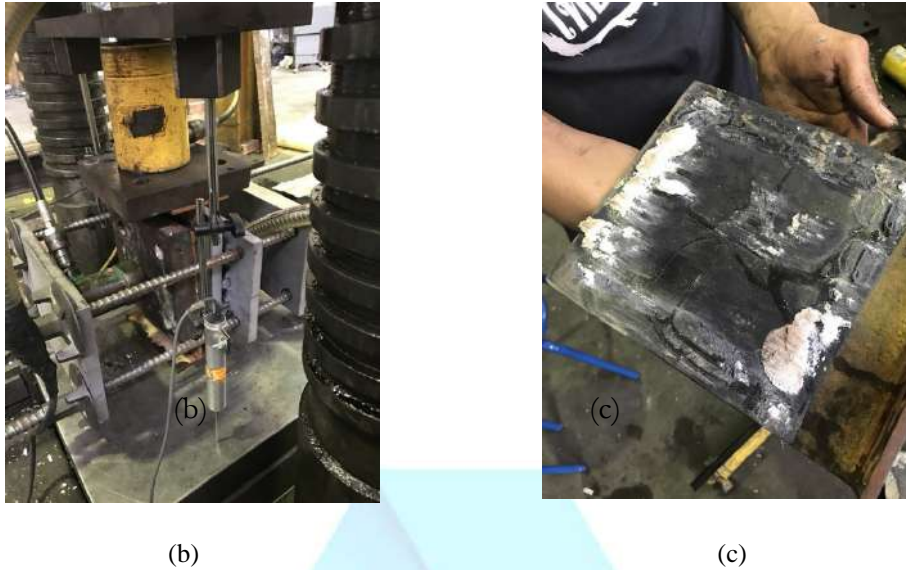


Figure 3: Compression-shear test; (a) Specimen dimensions; (b) Actual test setup; (c) Post-test rubber seal

3. Experimental result & discussion

Four dry joints have been tested with elastomeric bearings. Table 1 shows the final shear stress and shear modulus. It is calculated according to ASTM D 4014 [7]. Table 2 results show a positive relationship between the level of confinement and the level of rubber hardness to the final shear stress. The 2 MPa confinement produces final stresses of 6.27 percent and 27.29 percent higher than those of 1 MPa respectively for rubber hardness levels of 60 and 70. 70 hardness level causes final shear stress at 6.58 percent and 27.66 percent higher than 60 hardness level with confinement of 1 MPa and 2 MPa respectively. As shown in Figure 4 and Figure 5, the stress-strain curves for both levels of confinement show similar patterns. At the start, the slope is higher and slowly declines until it hits 100% strain.

Table 1 Experimental results of compression-shear test on joints

Specimen	Final shear stress*	Shear modulus**
	(MPa)	(MPa)
M1-60	0.95	2.71
M1-70	1.02	3.80
M2-60	1.01	2.71
M2-70	1.29	3.74

*final shear stress is the shear stress at 100% strain

**Shear modulus is calculated by taking the secant modulus from the point of 2% maximum stress to the point at 25% shear strain

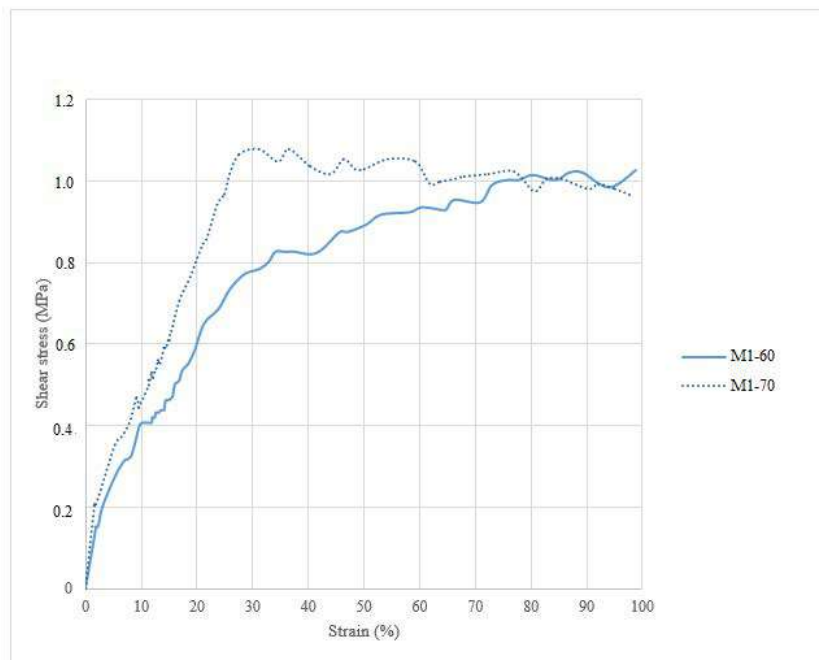


Figure 4: Shear stress-strain curve of elastomeric bearings with confinement of 1 MPa

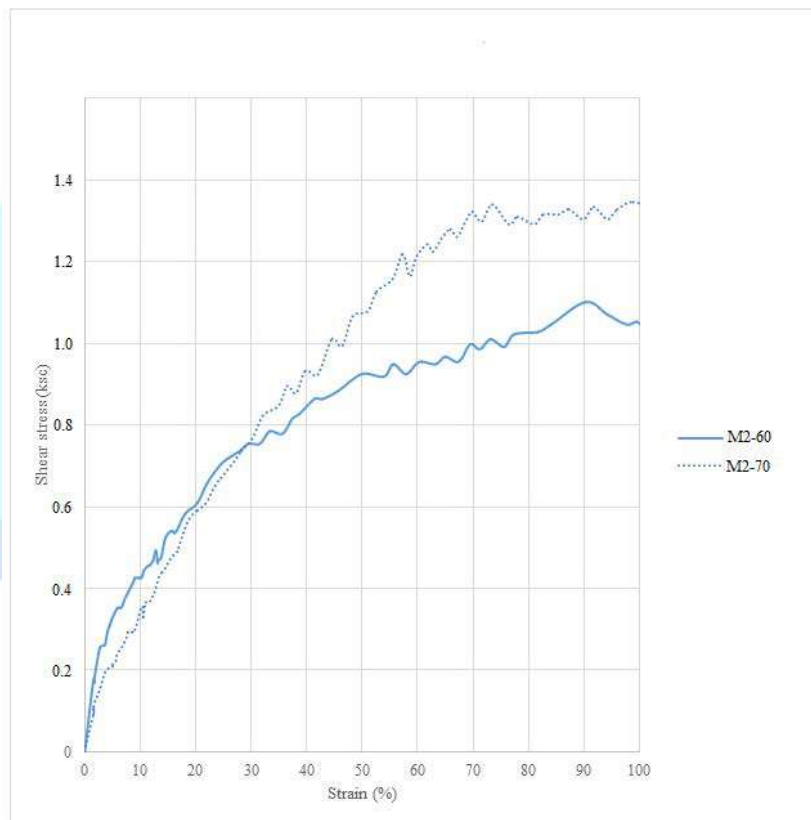


Figure 5: Shear stress-strain curve of elastomeric bearings with confinement of 2 MPa

Table 2: Results comparison to unseal joints by Zhou (2005)

Confinement MPa	Final shear stress		
	Mx-60 MPa	Mx-70 MPa	Unsealed joints MPa
1	0.95	1.02	0.68
2	1.01	1.29	1.47

*results by Zhou, X. (2005) [12]

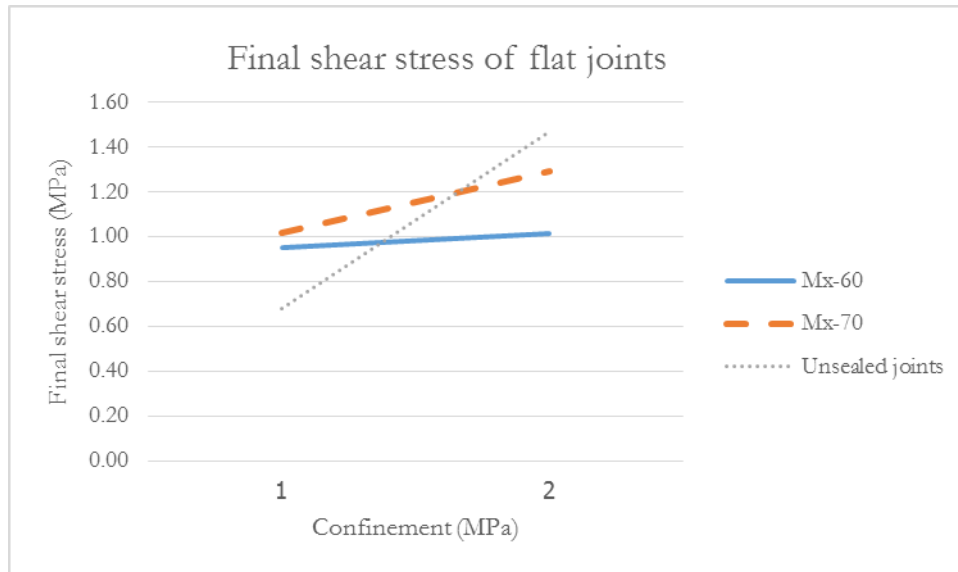


Figure 6: Final shear stress comparison

Our result is compared with four unsealed joints of Zhou (2005), as shown in table 2 and plotted in figure 6. The final shear stress of unsealed joints at 1-MPa confinement is lower than those with intermediates. Nevertheless, with confinement at 2 MPa, the result conversely shows that the final shear stress of unsealed joints are higher than those with intermediates. These two types of joints represent completely different shear mechanism. The shear stress in unsealed joints comes from mere friction. Until it slips, it can bear shear stress. The higher confinement contributes to increased friction. On the other side, there is no slip at joints in all experiments until they exceed 100 percent strain of straight joints with intermediates. Thus, in this system, the shear stress of flat joints with intermediates is extracted from shear resistance based on the properties of rubber itself.

4. Conclusion & limitation

This paper demonstrates the shear strength of rubber seals in joints and confirm the study of Xiao, W. Et al. (2017) that the rubber contributes substantial shear resistance to joints. Compare to unsealed joints, rubber seals unexpectedly provide higher shear resistance

than concrete-to-concrete surface at a confinement level. Hence, it is necessary to study mechanical properties of rubber seal further as it provides new applications to structures and cease the non-shear assumption of rubber seals. The limitation of this research is that only 2 average normal stress levels were concentrated in this paper. The compression-shear test should be reexamined to confirm the relationship between final shear stress and confinement.

5. References

1. Rasmussen, N. S.(1997). Concrete immersed tunnels – Forty years of experience. *Tunnelling and Underground Space Technology*, 12(1), 33-46.
2. Xiao, W. & Yu, H. & Yuan, Y. & Taerwe, L. & Xu, G. Compression-shear behavior of a scaled immersion joint with steel shear keys. *Tunnelling and Underground Space Technology*, 70, 76-88.
3. Stanton, J. F. & Roeder, C. W. Elastomeric bearings design, construction and materials. Transportation research board, National research council, Washington D. C., August, 1982.
4. Hu, Z. & Xie, Y. & Wang, J. Challenges and strategies involved in designing and constructing a 6 km immersed tunnel: A case study of the Hong Kong–Zhuhai–Macao Bridge. *Tunneling and Underground Space Technology*, 50, 171-177.
5. Zhou, X. & Mickleborough, N.C. Shear strength of joints in precast concrete segmental bridges. *ACI Structural Journal*, 102, January-February, 2005.
6. Thai Industrial Standard 951-2533. *Thai Industrial Standard, Ministry of Industry of Thailand*, 107, 1-9, July, 1990.
7. Standard specification for plain and steel-laminated elastomeric bearings for bridges. ASTM Standards. *American society for testing and materials*, 04.03, 409, Philadelphia, 1995.

PAPIdroid: A Risk Scoring of Android Malware Apps Based on Permissions and API Call

Hendrik Maulana Mardiyansyah, Eka Kurnia Sari, Imam Baehaki, Mohammad Agus Prihandono

Electrical Engineering Department, Universitas Indonesia, Indonesia

Email: hendrik.maulana@ui.ac.id

Abstract

The rapid growth of mobile device, specifically Android platform has consequences of the increasing of android malware. Detecting malicious behaviour of Andoird apps is important because it may steal user's sensitive data and even bank accounts. Many research conducted to achieve effective detection of malicious apps, most of them used permission analysis of Android apps. That method is less accurate because of malicious apps grow more complex and use obfuscation techniques to avoid antivirus detection. We develop a model that combine the permission and API Call assessment with five level steps analysis. The model reaches an accuracy of 95.7% to detect known malware apps with false positive rate as 0.4% and false negative rate as 0.6%

Keywords: Android security, malware detection, mobile security, obfuscation.

- *This research presented on 42th International Conference on Engineering, Technology and Applied Science (ETAS-42): Tokyo/Japan, January, 14th, 2020*

1. Introduction

Smartphones and tablets, or in general: mobile devices, become key features of the society and business activities. Up to 70% of web traffic comes from mobile devices [1]. Meanwhile, more than 10,000 malicious mobile apps blocked by antivirus per day[2]. This number shows that the increasing of the mobile device population is followed by the high numbers of malware as well. Malware authors seem more aggressive in digging up the new potential field to take benefit from criminal fraud activity.

McAfee reported a high growth of threats against internet-connected things and mobile devices throughout the second half of 2018. The hidden apps was become the first rank of threat and contribute around 30% in mobile attacks. They found TimpDoor malware family has a new spread strategy to reach the victim. They were contacting users directly via SMS to bypass the Google Play Store. This method can impact more victims than the older ones. Enter TimpDoor, an Android-based malware family was found as the new Mobile backdoor threat in March 2018. Starting in September 2018, McAfee noted that this threat has growth significant with more than 11 thousand infections [3].

Most of the users have limited knowledge of cybersecurity, they hardly to determine whether the current permission use is harmless or not. When installing apps, the permission warning interface is text-based [4]. This case makes users who have less cybersecurity knowledge, ignore the warning and accept all the permission warning when installing apps. Based on this experience, Yang Wang et al, conclude that the risk analysis based on the permission model in an android system becomes ineffective. Hence, it required a new model of risk assessment based on permission request patterns to facilitate the users in understanding and triggering the user's attention of the risk level of the permission request in order to prevent the spread of malware.

Detecting malware methods have been developed and improved every time by researchers and practitioners. However, the malware author also keeps improving their creativity in reforming malware penetration methods, such as an obfuscation technique. They use this technique to hide the malware payload from the malware detection tool such as reflection, emulator detection, application icon hiding. The custom obfuscation techniques generally using the method in loading native libraries, hiding exploits in package assets, truncating URLs, using encryption payload [5].

Several recommendations were made in this paper for android malware detection based on the risk rate calculation method. This method is using five steps and parameters in analyzing and calculating the risk rate to get a more comprehensive risk rate value. The comprehensive rate is expected able to increase the accuracy of malware detection.

2. Theory Related Topic

2.1 Obfuscation technique

The obfuscation is a technique that makes the program harder to understand[6]. For such a purpose, it converts a program to a new version while making them usefully to each other. This technique proposed for protecting the intellectual property of software developers, Obfuscation technique is widely used, in order to keep evade security scanners, malware developed into new generation through the obfuscation technique. It is important to study in detail the obfuscation techniques to effectively characteristic malware.

2.2 Static Analysis Tools

Static analysis is the procedure of analyzing software without executing the program. During static[7] analysis, the application is broken down by using reverse engineering tools and techniques, re-build the source code and algorithm that the application has created. Static analysis can be done through a program analyzer, debugger, and disassembler. Various static analysis techniques are RiskInDroid and Quark-Engine.

RiskInDroid[8] is a tool for quantitative risk analysis of Android applications written in Java used to check the permissions of the apps) and Python (used to compute a risk value based on apps' permissions). Quark-Engine is a tool for measuring risk analysis of android that are consists of five stages to see if the malicious activity is running. They are : permission request, native API call, combination of native API. calling sequence of native API. register handled by APIs. We are not only define malicious activities and their stages but also develop weights and thresholds for calculating the threat level of malware.

2.3 Dynamic Analysis Tools

Dynamic analysis is the procedure of analyzing software executed in a controlled environment. Dynamic techniques analyze the code during run-time. While these techniques are non-exhaustive, they have a significant advantage that only those instructions are analyzed that the code executes. Thus, dynamic analysis is immune to obfuscation attempts and has no problems with self-modifying programs. The question exists in which environment the sample code should be executed. Analyzing malware directly on the analyst's computer, which is probably connected to the Internet, could increase the risk that malicious code could easily escape and infect other machines. Running the executable in a virtual machine, such as one provided by VMware [9], is a popular choice. In this case, the malware can only affect the virtual PC and not the real one.

2.4 Risk Assessment Android

The purpose of the risk assessment is to provide a quantitative estimation software that can be characterized by combining the severity of the app that causes potential failure events to users and the probability of its occurrence [10]. For example, an application using geolocation may be malicious.

To assess the risk level of resource accesses, the activities of the apps monitored using application permission, API permission and the data result are calculated based on that feature. Our risk assessment mechanism uses calculation, addition, and provides users with a risk level of involved resource accesses.

2.5 Android API Call

The Android platform provides a framework API that Apps can use to interact with the underlying Android system. The framework API consists of a core set of packages and classes. We use the android system to monitor the combination native API call. Apps may invoke some APIs to access certain privacy information during execution. There are finding a cross reference and calling sequence of the native API and tracing the bytecode register.

3. Related Works

There are several kinds of research related to malware scoring. Yang Wang et al. [4] proposed DroidRisk, a quantitative method to compute the risk of Android applications and permissions. The risk score is calculated based on the potential impact as well as the type of permission whether it is normal permission or dangerous permission. It used a static weight to represent the impact of permission-based on the permission category, 1 for normal permission category and 1.5 for the dangerous permission category.

Dini et al. [11] introduced MAETROID, a framework that evaluates the applications requested permissions along with its metadata. The permission risk score is computed by assigning a static weight to each requested permission based on the permission threat category. However, the authors did not provide any empirical evaluation and analysis of their proposed framework.

Alshehri et al. [12] proposed PUREDroid, a risk assessment method that can be used to increase the user's awareness of the risk involved with granting permissions to Android applications. This model has shown that permissions that perform suspicious activities are assigned to high-risk scores unlike those of normal activities.

Li et al. [13] introduced SigPID, a malware detection system based on permission usage analysis to cope with the rapid increase in the number of Android malware. It used three

levels of cropping by mining the permission data to identify the most significant permissions that can be effective in distinguishing between benign and malicious applications. Then it utilizes machine-learning based classification method to classify different families of malware and benign applications.

Merlo et al. [8] evaluated RiskInDroid, a machine Learning-based Risk Analysis on Android. RiskInDroid approach based on four sets of permission: Declared Permissions, Exploited Permission, Ghost Permission, and Useless permission.

Gates et al. [14] introduced a new method to generate risk signals based on the permissions requested by an application. It aims to provide users with feedback about why the application is risky. The risk score is calculated using different Bayesian probabilistic models to satisfy three goals, namely, monotonicity, coherence, and ease.

Deypir [15] proposed a new approach to calculate the security risk score of Android permissions based on the concept of information theory and entropy. For each permission, the information gain is computed by calculating the entropy of the entire used dataset and the entropy of the permission within the dataset. In this approach, the higher risk score is assigned to the permission that is more informative. Yet, the author neglected the application categories of the analyzed applications, which negatively affect the risk score since applications from different categories portray different functionality. In addition, information gain has symmetric property, which can incorrectly assign a high-risk score to permission that is mostly used by benign applications.

4. Methods

This chapter covers our methods for exploring the risk in Android apps. We developed six steps to see risk in apps. First, we rank the permission that used by the apps from most to least risky. Second, we analyze the combination of a native API call. Third, the sequence of API calls ranked. Fourth, analyze the sequence of calling API. Fifth, Analyze the API that handles the same register. Sixth, we develop weights and thresholds for calculating the threat level. To avoiding obfuscation techniques, we provide the order theory. There are finding the cross reference and calling sequence of the native API and tracing the bytecode register.

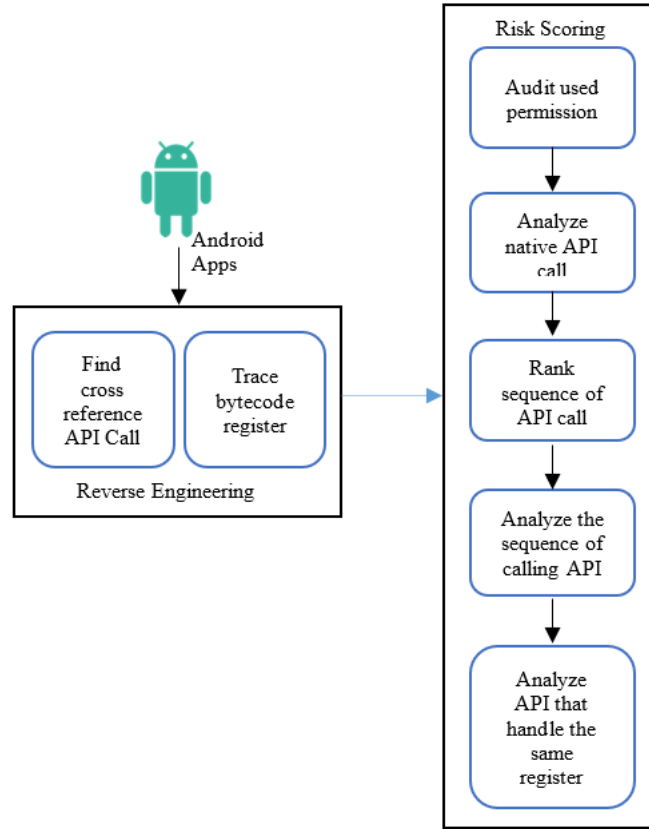


Figure 1. Proposed scheme

4.1 Risk Score Based on Permission

We follow the NIST guide for risk assessment. We assumed that permission used by an application is independent, so the risk level of an application can be defined as:

$$R_p = L_p \times I_p \quad (1)$$

where R_p is the risk level of application based on permission, L_p is the likelihood, and I_p is the impact of permission. To calculate the likelihood, we define it as the conditional probability defined by Bayes rule as shown below:

$$L_p = \frac{P(p_i | A \text{ is malware}) \times P(A \text{ is malware})}{P(p_i)} \quad (2)$$

where $P(p_i | A \text{ is malware})$ is the probability that malware requests p_i permission, $P(A \text{ is malware})$ is the probability that an app is a malware, and $P(p_i)$ is the probability of an app requests p_i permission. Because the actual level of impact caused by permissions is hard to obtain, we use the ROC (Receiver Operating Characteristic) curve.

4.2 Risk Score Based on API Call

Basically, we use the API analysis to extend the permission-based risk assessment. We divide the analysis into five steps as mentioned before. To calculate the risk level based on API analysis we used this formula:

$$Rb = F(A_i) + F(A_c) + F(A_s) \quad (3)$$

where Rb is the risk score based on API call, $F(A_i)$ is the feature score of the API call, $F(A_c)$ is the feature score of the combined API call, and $F(A_s)$ is the feature score of the sequence API call. $F(A_i)$ use Correlation Based Feature Selection (CFS) can be defined as follow:

$$F(A_i) = \frac{n\bar{r}_{cf}}{\sqrt{n + n(n-1)\bar{r}_{ff}}} \quad (4)$$

where n is features, $n\bar{r}_{cf}$ is the mean feature class-correlation, and \bar{r}_{ff} is average feature correlation.

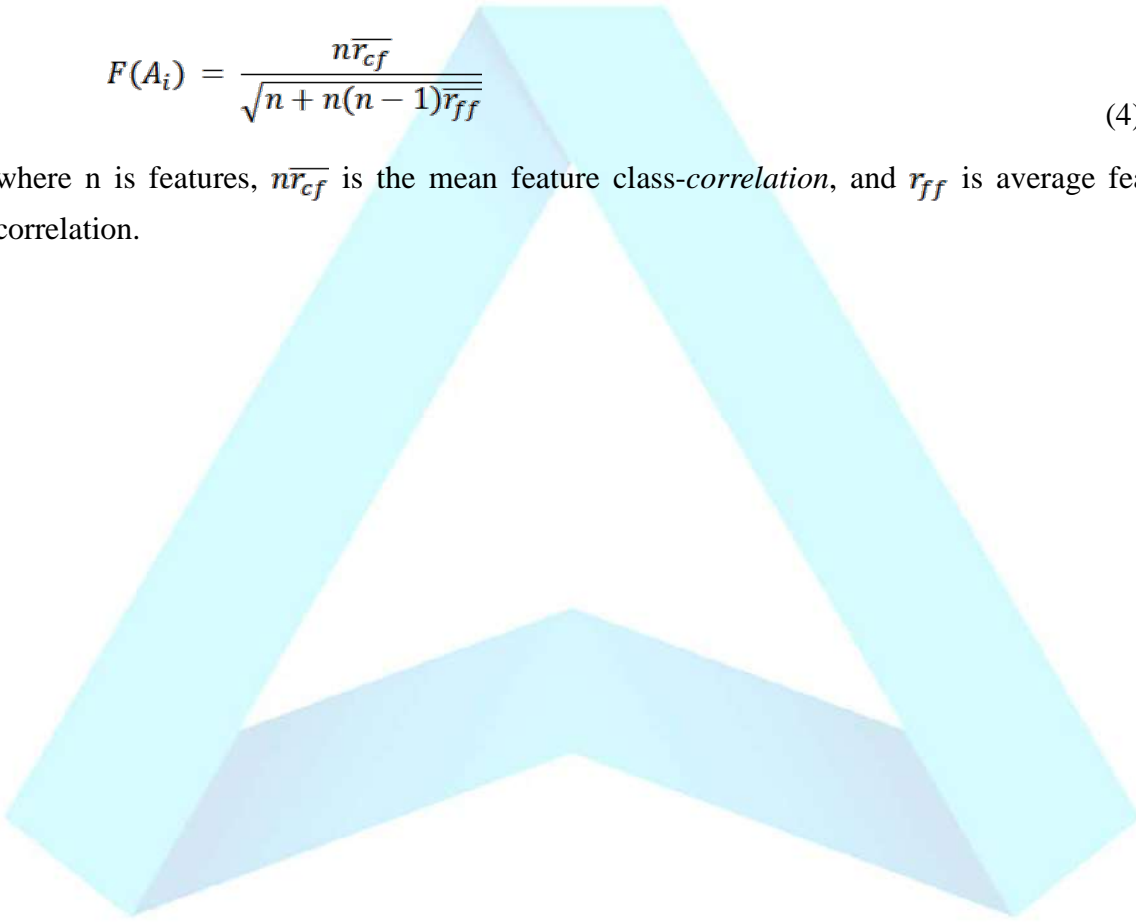


Table 1. API Call score using the CFS method

Feature (API Call)	Score
getSubscriberId	1
getSimSerialNumber	2
getInstalledPackages	3
getServiceCenterAddress	4
getLine1Number	5
getDeviceId	6
get_accounts	7
getDataActivity	8
getActivityNetworkInfo	9
getSupplicantState	10
getNetworkType	11
getSimOperator	12
getCallState	13
getConnectionInfo	14
getSimState	15
abortBroadcast	16

$F(A_c)$ can be calculated from the sum of each API call score. Then $F(A_s)$ can be calculated with the formula:

$$F(A_s) = \Sigma(P(A_c) \times F(A_c)) \quad (5)$$

where the $P(A_c)$ is the probability of API call combination.

4.3 Total Risk Score

Our method calculates the risk score with a combination of permission-based and API Call based. We define it as:

$$R_T = R_p + R_b \quad (6)$$

where R_T is the total risk score. Then we map the total score into three classifications of risk, there are low, moderate, and high risk.

Tabel 2. Risk score classification

Classification	Score
Low	0 - 45
Moderate	45 - 75
High	> 75

5. Result

5.1 Dataset

Dataset used in this research consist of 6488 benign apps and 6437 malware samples. We collect the apps from APKPure, PlayStore, and Github.

5.2 Performance

To prove our scheme, we tested it on the dataset to classify the apps as benign or malware. Simulation runs in a Python environment to disassemble the APK and then calculate the risk score.

Figures 2. shows the top 15 requested permission in the benign dataset and malware dataset. INTERNET got the highest rank in the most frequently used permission by both datasets. ACCESS_NETWORK_STATE and ACCESS_WIFI_STATE also got high rank because it related to the INTERNET.

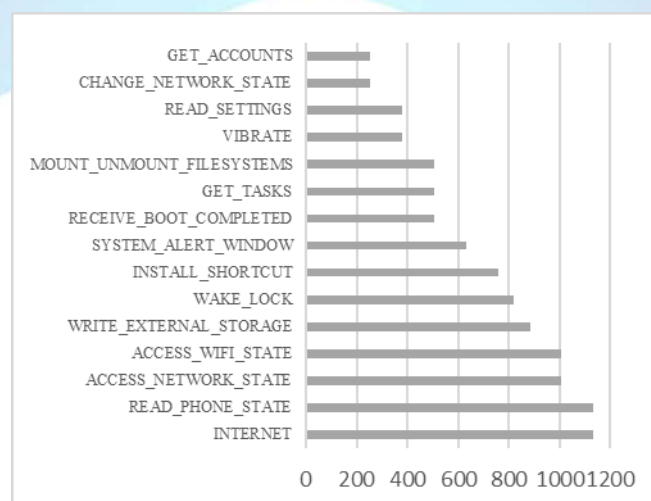


Figure 2. Top permissions used in the dataset

Figure 3. shows that `getSubscriberId` become mostly used API call. This function request for unique subscriber ID or International Mobile Subscriber Identity that uniquely identifies every user of a cellular network

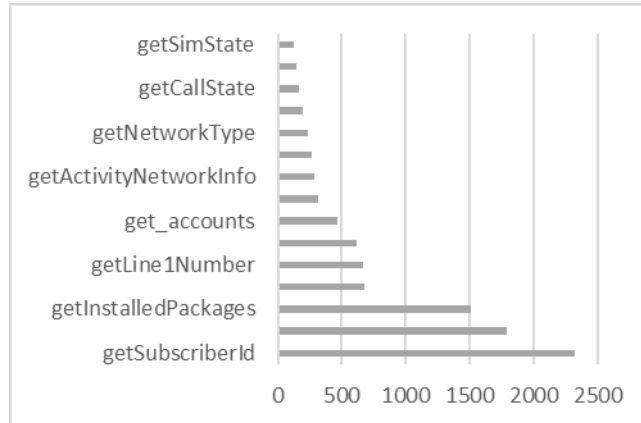


Figure 3. Top API Call used in the dataset

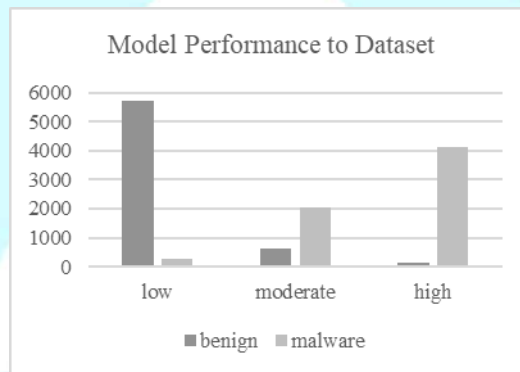


Figure 4. Model performance to the dataset

Figure 4 shows that our proposed model performs well to classify the apps in the dataset. From the benign list, our model detects 5711 low-risk benign apps and from the malware list, it detects 4412 high-risk malware apps.

5.3 Evaluation

Several kinds of literature provide many evaluation metrics that can be used in this scenario. We choose the accuracy rate (Acc) and error rate (Err) to evaluate the performance of our model.

$$Acc = \frac{n_{ben \rightarrow ben} + n_{mal \rightarrow mal}}{n_{ben \rightarrow ben} + n_{mal \rightarrow mal} + n_{ben \rightarrow mal} + n_{mal \rightarrow ben}} \quad (7)$$

$$Err = \frac{n_{ben \rightarrow mal} + n_{mal \rightarrow ben}}{n_{ben \rightarrow ben} + n_{mal \rightarrow mal} + n_{ben \rightarrow mal} + n_{mal \rightarrow ben}} \quad (8)$$

In addition, we also calculate the true positive rate (TPR), true negative rate (TNR), false positive rate (FNR), and precision (p) as below:

$$TPR = \frac{n_{mal \rightarrow mal}}{n_{mal \rightarrow mal} + n_{mal \rightarrow ben}} \quad (9)$$

$$TNR = \frac{n_{ben \rightarrow ben}}{n_{ben \rightarrow ben} + n_{ben \rightarrow mal}} \quad (10)$$

$$FPR = \frac{n_{ben \rightarrow mal}}{n_{ben \rightarrow ben} + n_{ben \rightarrow mal}} \quad (11)$$

$$FNR = \frac{n_{mal \rightarrow ben}}{n_{mal \rightarrow ben} + n_{mal \rightarrow mal}} \quad (12)$$

$$p = \frac{n_{mal \rightarrow mal}}{n_{ben \rightarrow mal} + n_{mal \rightarrow mal}} \quad (13)$$

where the $n_{ben \rightarrow ben}$ is the number of benign apps that classified correctly as Benign, $n_{ben \rightarrow mal}$ is the number of benign apps that classified as malware, $n_{mal \rightarrow mal}$ is the number of malware apps that classified correctly as malware and $n_{mal \rightarrow ben}$ is the number of malware apps that classified as benign.

Table 3. Evaluation results

Acc	Err	TPR	TNR	FPR	FNR	p
0,9578	0,0421	0,9356	0,9745	0,0482	0,0644	0,9650

6. Discussion

We argue that our approach for exploring risk in the Android app is better than other methods, especially with RiskInDroid. As shown in Table 3, the accuracy rate of our model is

0,9578; and if we compare it with an accuracy rate of the RiskInDroid model, as shown in table 4, our model is 12.79% more accurate than RiskInDroid model.

Table 4. Accuracy rate calculated by probabilistic methods and RiskInDroid [8]

Static Impacts	Dynamic Impacts	RiskInDroid
0,7129	0,8610	0.8424

The key difference is: we reverse-engineering the app by finding cross-reference API call and tracing bytecode register; we score risk by auditing used permission, analyzing native API, ranking sequence of API call, analyzing the sequence of calling API, analyzing API that handles the same register, provide the order theory to avoiding the obfuscation techniques.

7. Conclusion and Future Work

In this paper, we provide an effective and accurate approach to detect malware apps in the Android operating system. We applied five levels of scoring based on apps permissions and API calls. Our method has a high detection rate for malware apps and benign apps. It's better from another permission-based risk scoring. To get better accuracy, we will conduct further research in evading obfuscation techniques because it is important to accurately trace the API call used in Android.

8. References

1. Samantha Ann Schwartz (2017), 70% of internet traffic comes from mobile phones [online] CIO Dive, Available at <https://www.ciodive.com/news/70-of-internet-traffic-comes-from-mobile-phones/510120/> [accessed at 5 Dec 2019]
2. Brigid O'Gorman, Candid Wueest, Dick O'Brien, Gillian Cheary, Hon Lau, John-Paul Power, Mayee Corpin, Orla Cox, Paul Wood, Scott Wallace, Internet Security Threat Report, Volume 24 | February 2019, Symantec, California, United States of America
3. Raj Samani, Gary Davis. Mobile Malware Continues to Increase in Complexity and Scope. McAfee Mobile Threat Report, March 2019, McAfee, California, United States of America
4. Yang Wang, Jun Zheng, Chen Sun, Srinivas Mukkamala. Quantitative Security Risk Assessment of Android Permissions and Applications. 27th Data and Applications Security and Privacy (DBSec), Jul 2013, Newark, NJ, United States. pp.226-241,

ff10.1007/978-3-642-39256-6_15ff. fhal-01490707

5. Axelle Apvrille, Ruchna Nigam. Obfuscation in Android malware, and how to fight back. *Virus Bulletin*. Jul 2014. Fortinet, France. Available at <https://www.virusbulletin.com/virusbulletin/2014/07/obfuscation-android-malware-and-how-fight-back> [accessed at 20 Dec 2019]
6. A. Balakrishnan and C. Schulze, "Code Obfuscation Literature Survey," <http://pages.cs.wisc.edu/~arinib/writeup.pdf>, 2005.
7. Bergeron, J., Debbabi, M., Desharnais, J., M., E., M., Lavoie, Y., & Tawbi, N. (2001). Static Detection of Malicious Code in executables programs. *International Journal of Req Engineering*
8. Alessio Merlo and Gabriel Claudiu Georgiu, "RiskInDroid: Machine Learning-based Risk Analysis on Android," 2017.
9. VMware: server and desktop virtualization, 2006. <http://www.Vmware.com/>
10. G. Hogben and M. Dekker, "Smartphones: Information security risks, opportunities and recommendations for users," *European Network and Information Security Agency*, vol. 710, no. 01, 2010.
11. Gianluca Dini, Fabio Martinelli, Ilaria Matteucci, Marinella Petrocchi, Andrea Saracino, and Daniele Sgandurra. 2018. Risk analysis of Android applications: A user-centric solution. *Future Generation Computer Systems* 80 (2018), 505–518
12. Alshehri et al. PUREDroid: Permission Usage and Risk Estimation for Android Applications. *ICISDM 2019 Proceedings of the 2019 3rd International Conference on Information System and Data Mining*. Pages 179-184
13. Li et al. SigPID: significant permission identification for android malware detection. 2016 11th International Conference on Malicious and Unwanted Software (MALWARE)
14. Mahmood Deypir. 2018. Entropy-based security risk measurement for Android mobile applications. *Soft Computing* (04 Aug 2018). <https://doi.org/10.1007/s00500-018-3377-5>
15. C. S. Gates, N. Li, H. Peng, B. Sarma, Y. Qi, R. Potharaju, Nita-Rotaru, and I. Molloy. 2014. Generating Summary Risk Scores for Mobile Applications. *IEEE Transactions on Dependable and Secure Computing* 2014. <https://doi.org/10.1109/TDSC.2014.2302293>

Development of Travel Demand Models under Earthquake by Using Spaghetti and Meatballs Method and Four-Step Transportation Model

Jessada Pochan^{ab}, Preda Pichayapan^{bc}, Kriangkrai Arunotayanun^{bc}

^aDoctoral Degree Program in Civil Engineering, Chiang Mai University, Thailand

^bDepartment of Civil Engineering, Faculty of Engineering, Chiang Mai University, Thailand

^cExcellence Center in Infrastructure Technology and Transportation Engineering, Chiang Mai University

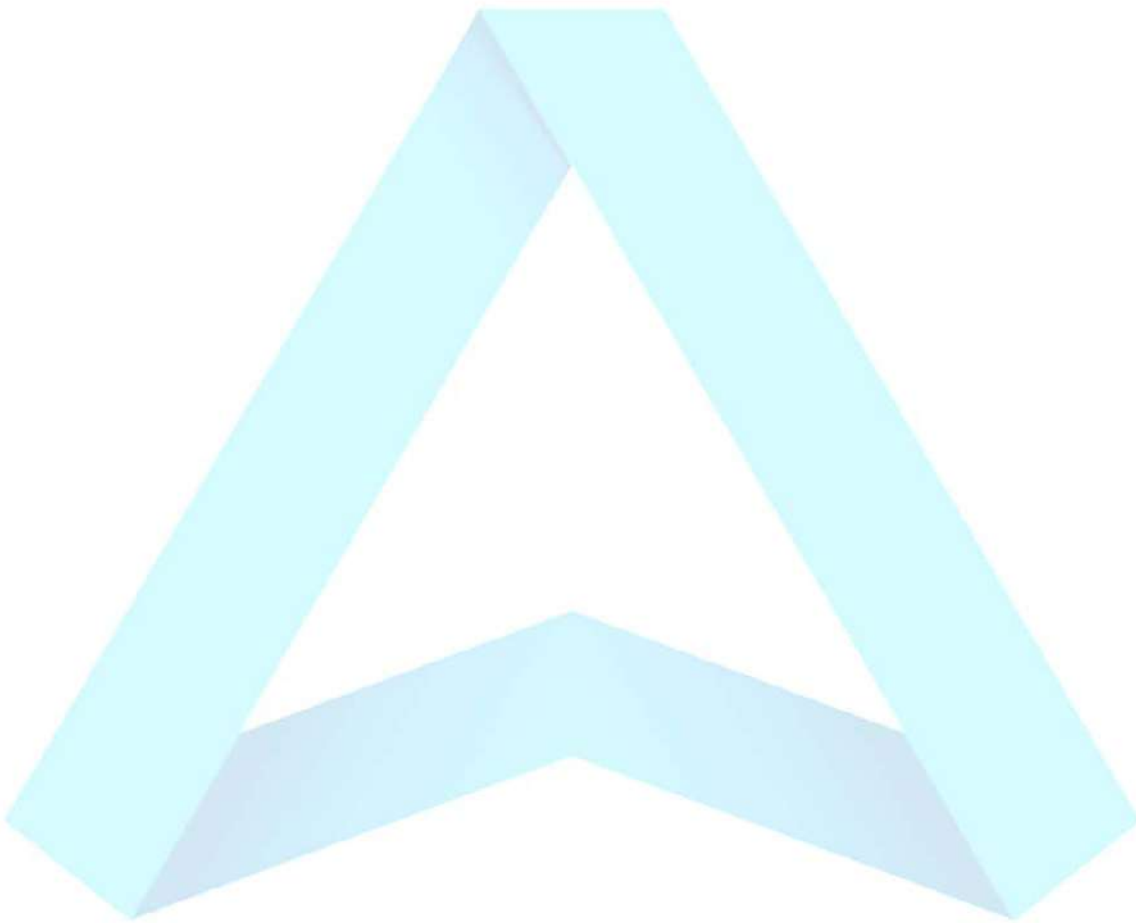
Email Address: preda@eng.cmu.ac.th

Abstract

This paper presents a modeling framework for forecasting travel demand under earthquake, developed through perspective of transportation engineering. The proposed framework consists of two sequential steps: 1) Seismic risk analysis, to evaluate the vulnerability of both road network and area-covering disruptions, using the spaghetti and meatballs method, which is a geographic information system (GIS) based analytical approach enriched with historical earthquake statistics and earthquake fault data; and 2) Travel demand analysis, to forecast travel demand, travel behavior, travel pattern, and traffic volume, using the four-step transportation model developed based on field traffic survey data and seismic risk analysis data. To evaluate model mechanism and performance, a preliminary model was then applied to the simulated geographical area with simulated road network. As the result, the traffic conditions before and after the earthquake were different. The traffic condition after the earthquake was worse than before the earthquake. In case of an hour after earthquake, level of service (LOS) changed from B to D level (up 2 levels), where traffic volume, vehicle kilometers of travel (VKT), and vehicle hours of travel (VHT) increased approximately 18.36%, 19.11%, and 106.62%, but average speed decreased about 42.35%. Moreover, In case of a day after earthquake, LOS changed to C level (up 1 level), where traffic volume, VKT, VHT, and average speed decreased approximately 23.35%, 24.93%, 6.43%, and 19.77%, respectively. The resulting model can provide government and related agencies profound information in planning and developing either pre- or post-disaster operations.

Keywords: Travel Demand Prediction, Spaghetti and Meatballs Method, Four-Step Transportation Model

-
- *This research presented on 42th International Conference on Engineering, Technology and Applied Science (ETAS-42): Tokyo/Japan, January, 14th, 2020*



1. Introduction

Nowadays, world society has been faced to many natural and man-made disasters that cause massive economic and social damage as well as loss of lives every year [1]. The frequency and intensity of natural disasters have also been increasing over the past decades [1]. The natural disasters are often unpredictable [2] such as flood disaster [3, 4], tsunami disaster [5], landslide disaster [6], hurricane evacuation [2], earthquake disaster [7-9], and etc. Thus, planning for response to different natural disasters, including earthquake, has become an important aspect of urban management [10].

Earthquakes often result in severe human loss and intensive economic and social problems [10]. Moreover, the earthquake caused mass evacuation activities owing to considerable damage to buildings and urban infrastructure [11-14]. Therefore, travel demand behavior prediction in disaster scenarios is crucial for various recovery efforts, including the planning of locations and capacities of evacuation shelters, and the allocation of various emergency supplies [15-17].

During the last few decades, Geographic information systems (GIS) have increasingly popular technique for urban planning and design practice [18]. The main technique of GIS is to integrate a range of geographical information into a single analytical model, in which diverse data are georeferenced to cartographic projections [18]. The applications of GIS can be found in many research areas. For examples, Pence, et al. [19] applied GIS for probabilistic risk assessment to emergency preparation, planning, and response for severe nuclear power plant accidents. Putri and Maryono [20] investigated an evacuation route based on least cost path for Mount Merapi hazard in Mriyan-Boyolali, Indonesia, by using an ArcGIS raster analysis. Jiang, et al. [21] developed decision tools using GIS based on a real-time risk assessment on emergency environmental decision support system for response to chemical spills in river basin. Trozzi, et al. [22] applied the GIS and decision support system to emergency planning in the risk areas of industrial plants at the Lombardy region in Italy. However, in case of earthquake disasters, several vehicles of each mode of transportation between the traffic analysis zones should be considered together with the GIS.

Many years ago, the conventional four step travel demand model has supported the policy makers to make the decisions for transportation programs and projects [23, 24]. The number of vehicles of each mode of transportation between the traffic analysis zones has been predicted over a period [23, 25]. Many research works focused on four step travel demand model have been applied for various urban and transportation policy [23, 24], but they have not been found when that model has been applied to pre or post disaster operations using "four step travel demand" and "disaster" or "earthquake" as keywords searched in Scopus database.

2. Methodology

This paper presents a modeling framework for forecasting travel demand under earthquake. The models developed by using spaghetti and meatballs method and four-step transportation model for evaluate the vulnerability of both road network and area-covering disruptions, and forecast travel demand, travel behavior, travel pattern, and traffic volume, respectively. The proposed framework consists of two sequential steps: 1) Seismic risk analysis and; 2) Travel demand analysis, as shows in Figure 1. However, the analysis of both steps requires the development of simulated geographical area and simulated road network of the study area first.

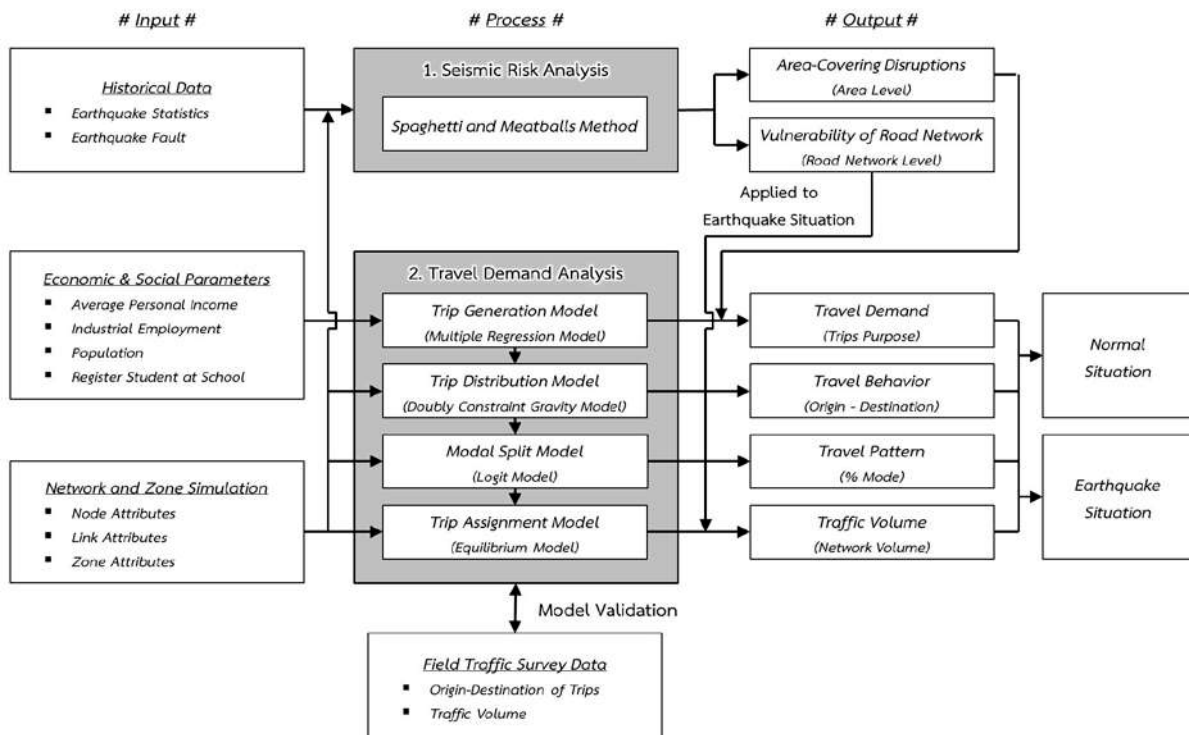


Figure 1: Conceptual Framework of Developing Travel Demand Models under Earthquake

2.1 Seismic Risk Analysis

Seismic risk analysis aims to evaluate the vulnerability of both road network and area-covering disruptions, using the spaghetti and meatballs method, which is a geographic information system (GIS) based analytical approach enriched with historical earthquake statistics and earthquake fault data. The Process of spaghetti and meatballs method was performed by Whirlpool; a geometric processor originally designed for polygon overlay [26-27], which was used to calculate the number of overlapping polygons. There are three steps to develop as following:

- 1) Identify the center of the historical earthquake and the earthquake fault data on the simulated geographical area and the simulated road network
- 2) Identify the area affected by each historical earthquake by using the relationship between magnitude and distance affected [28].
- 3) Evaluate the vulnerability of both road network and area-covering disruptions by using the spaghetti and meatballs method under the hypothesis that "the most overlapping area is the highest seismic risk in the study area"

2.2 Travel Demand Analysis

Travel demand analysis aims to forecast travel demand, travel behavior, travel pattern, and traffic volume of the study area, both normal situation and earthquake situation, using the four-step transportation model developed [29-31] based on field traffic survey data and seismic risk analysis data. The developed models require the calibration to consistent with local traffic conditions of the study area, according to acceptable criteria of UTPS highway network development guide [32].

1) Trip Generation Model

The trip generation model in this research consists of two sub-models: Trip production model and Trip attraction model, which is the developed model according to multiple linear regression analysis by finding the relationship between the travel demands, obtained from the field traffic surveys, and socioeconomic characteristics in the area [29, 33], such as average personal income, industrial employment, population, register student at school, and etc. Moreover, the model also considered the reduction of travel demand after earthquake, which used simulating the travel demand decision of people in the area, according to the principles of binary logistic regression analysis, as shown in the equation (1) and (2). However, the trip generation models is the sum of all trips purpose in the study area, which consists: the home-based work trips (HBW), the home-based school trips (HBS), the home-based other trips (HBO), the non-home-based trips (NHB) and the return home trips (RH).

$$P_{i(Purpose)} = \left[C_P + \sum_{j=1}^n (a_j X_{j(i)}) \right] \cdot \frac{I}{I + e^{-\left[D_P + \sum_{k=1}^m (g_k Z_{k(i)}) \right]}} \quad (1)$$

$$A_{i(Purpose)} = \left[C_A + \sum_{j=1}^n (b_j X_{j(i)}) \right] \cdot \frac{I}{I + e^{-\left[D_A + \sum_{k=1}^m (h_k Z_{k(i)}) \right]}} \quad (2)$$

Where,

- e = Irrational number ≈ 2.7182818
- $X_{1(i)}, \dots, X_{n(i)}$ = Socioeconomic variables of zone i
- a_1, \dots, a_n = Coefficients of trips production
- b_1, \dots, b_n = Coefficients of trips attraction
- $Z_{1(i)}, \dots, Z_{m(i)}$ = Earthquake variables of zone i
(magnitude earthquake scale, risk level, and etc.)
- $g_1, \dots, g_m, h_1, \dots, h_m$ = Logistic regression coefficients
- C_p, C_A, D_p, D_A = Constant

2) Trip Distribution Model

The trip distribution model in this research developed the model according to the principles of doubly constrained gravity model, which is the most popular in transportation planning [29]. The gravity model illustrates the interaction between two locations declines with travel time increasing between them, but is positively associated with the amount of activity at each location [33], like Newton's gravitational law [29]. The rate of decline of the interaction called the impedance or friction factor, as shown in the equation (3).

$$T_{ij} = \alpha_i \cdot \beta_j \cdot P_i \cdot A_j \cdot F(t_{ij}) \quad (3)$$

Where,

- T_{ij} = Trips between origin i and destination j
- α_i, β_j = Balancing factors of i and j
- P_i = Trips production at i
- A_j = Trips attraction at j
- $F(t_{ij})$ = Impedance or friction factor between i and j

3) Modal Split Model

The Modal Split model in this research developed the model according to the principles of logit model, which considered the utility functions of travelers received from each alternative [34]. The mode that considered in the model consisted passengers car, truck. Mathematically, the modal split model takes the form in the equation (4).

$$P_n(i) = \frac{e^{U_{in}}}{\sum_{j \in c_m} e^{U_{jn}}} \quad (4)$$

Where,

- $P_n(i)$ = Probability of individual n choosing mode i
- U_m = Utility function for modes i of individual n
- c_m = Number of total modes
- j = Choice mode j

4) Trip assignment model

The trip assignment model in this research developed the model according to the principles of user equilibrium method, which is giving the exact solution. The method is developed based on Wardrop's first principle, which states that no driver can unilaterally reduce his/her travel costs by shifting to another route. Moreover, the model also considered vulnerability of road network after earthquake, which affected to reduction of road capacity and delay in travel time [35]. Mathematically, the trip assignment model takes the form in the equation (5) and (6):

$$\text{Min} \sum_{a \in A} \int_0^{V_a} t_a(\omega) d\omega \quad (5)$$

$$t_a = t_0 \cdot \left(1 + \alpha \cdot \left(\frac{V_a}{C_a} \right)^\beta \right) \quad (6)$$

Where,

- t_a = Travel time on link a
- t_0 = Travel time on link a (at free-flow speed)
- V_a = Traffic volume on link a
- C_a = Capacity on link a
- α, β = Coefficients

3. Case Study

To evaluate model mechanism and performance, a preliminary model was then applied to the simulated geographical area with simulated road network. Developing the network and zone simulation divided structure into 3 layers: 1) Zones layer or boundary 2) Node and centroid layer or point; and 3) Link layer or connector. The zones layer consist the attribute about boundary, area, average personal income, industrial employment, population, and register student at school. The attribute about GIS coordinates (X/Y) included in the node and centroid layer. In the part of the link layer, attribute consist distance, number of number of lane, traffic volume capacity, and free-flow speed. Moreover, each links are connected to the nodes and centroids of the zone, which is the linkage of trips production and trips attraction between those zones. Moreover, a case study divided the internal and external area into 28 zones and 4 zones, respectively. The road network in the study area was a grid line with size of 10 x 10 kilometers, located in the area as shown in Figure 2.

However, developing the travel demand models of study area was analyzed by three scenarios: 1) situation without earthquake; 2) situation after earthquake (1 hour); and 3) situation after earthquake (1 day), with assume that the Richter magnitude scale was 6. The historical earthquake statistics and earthquake fault data of case study was assumed as shown in Figure 3.

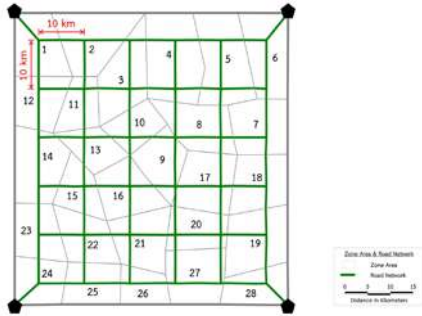


Figure 2: Simulated Geographical and Simulated Road Network

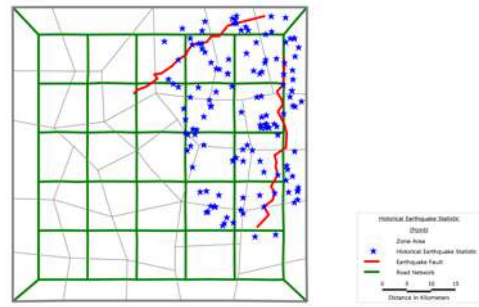


Figure 3: Historical Earthquake Statistics and Earthquake Fault Data

4. Results

The results of the development and application of models with the case study were as follows:

4.1 Results of Seismic Risk Analysis

The results of seismic risk analysis by the spaghetti and meatballs method, which used historical earthquake statistics and earthquake fault data was shown in Figure 4. In the part of Figure 5 and 6 demonstrated the area-covering disruptions and vulnerability of road network, respectively.

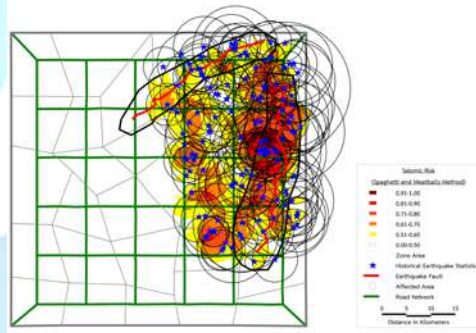


Figure 4: Seismic Risk Analysis

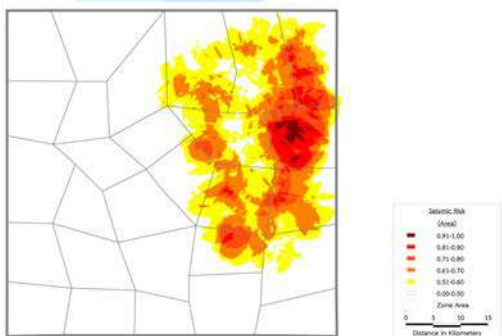


Figure 5: Area-Covering Disruptions

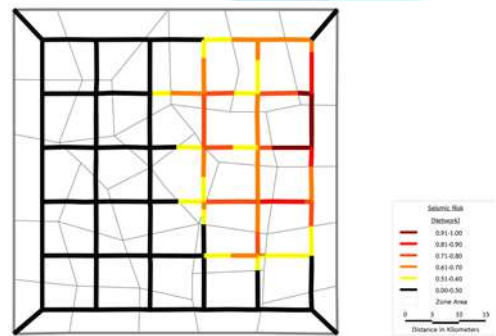


Figure 6: Vulnerability of Road Network

4.2 Results of Travel Demand Analysis

The results of travel demand analysis by the four-step transportation model, which used field traffic survey data and seismic risk analysis was shown in Figure 7 to 9 and Table 1.

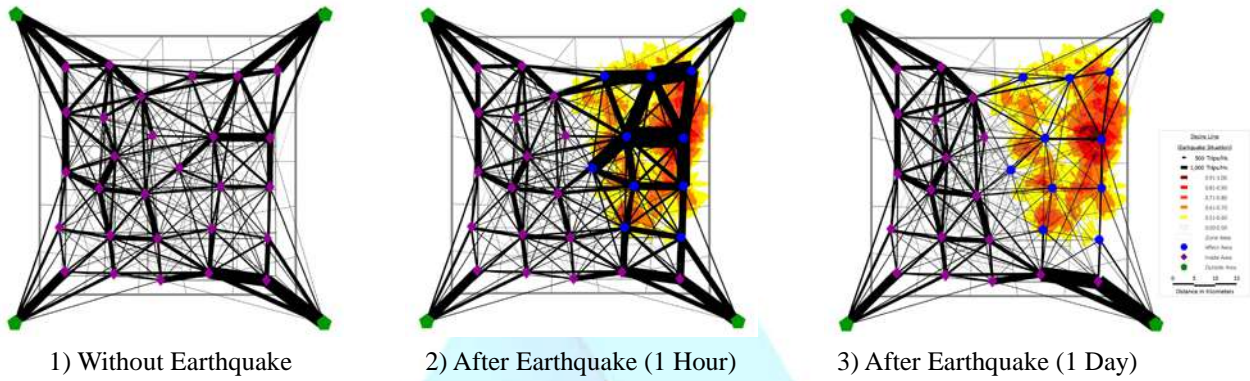


Figure 7: Travel Demand and Travel Behavior (Desire Line in Peak Hour)

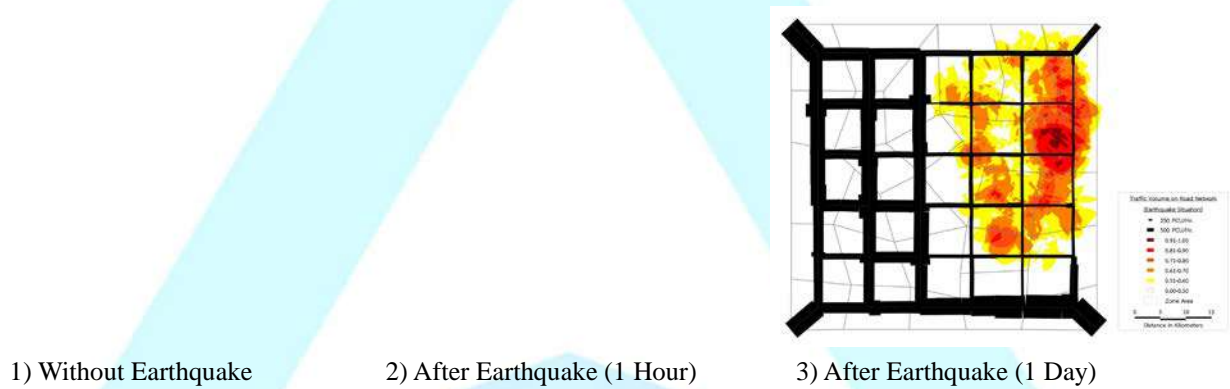


Figure 8: Traffic Volume on Road Network (Flow Diagram in Peak Hour)

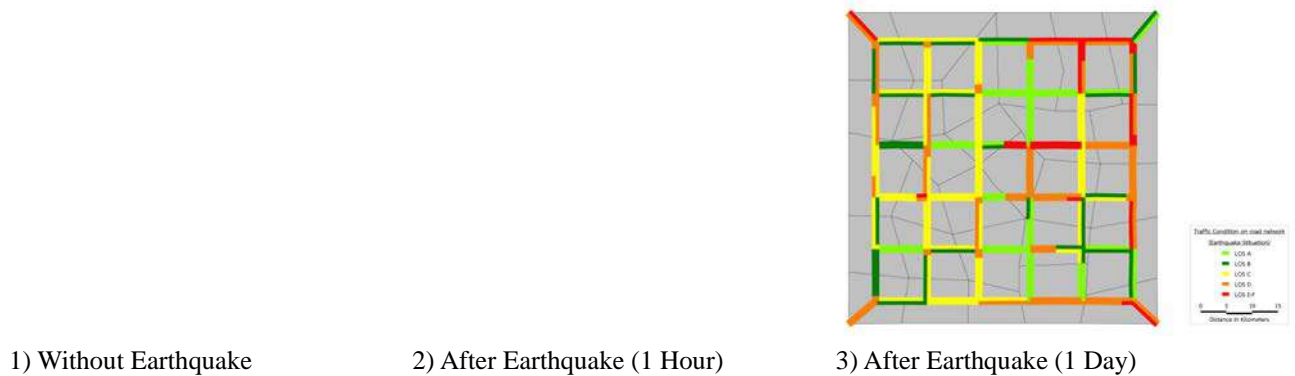


Figure 9: Traffic Condition on Road Network (Level of Service: LOS in Peak Hour)

Table 1: Summary of Overall Traffic Condition in Peak Hour

Traffic Condition (Overall)	Unit	Scenarios				
		Without Earthquake	After Earthquake (1 Hour)		After Earthquake (1 Day)	
			Value	Diff. (%)	Value	Diff. (%)
1) Traffic Volume	PCU/Hr.	54,679	64,719	+18.36	41,911	-23.35
2) Vehicle Kilometers of Travel (VKT)	PCU-Km./Hr.	1,036,705	1,234,871	+19.11	778,288	-24.93
3) Vehicle Hours of Travel (VHT)	PCU-Hr./Hr.	13,974	28,873	+106.62	13,076	-6.43
4) Average Speed	Km./Hr.	74.19	42.77	-42.35	59.52	-19.77
5) Level of Service (LOS)	-	LOS B	LOS D	Up 2 Level	LOS C	Up 1 Level

Remark: PCU is passenger car unit

The results of travel demand model analysis in three scenarios showed that travel demand, travel behavior and traffic conditions before and after the earthquake were different. Before the earthquake, the study area had overall level of service (LOS) in peak hour at B level, with traffic volume equal to 54,679 PCU/Hr., vehicle kilometers of travel (VKT) equal to 1,036,705 PCU-Km./Hr., vehicle hours of travel (VHT) equal to 13,974 PCU-Hr./Hr., and average speed equal to 74.19 Km./Hr..

However, the traffic condition after the earthquake was worse than before the earthquake. In case of an hour after earthquake, LOS changed from B to D level (up 2 levels), where traffic volume, VKT, and VHT increased approximately 18.36%, 19.11%, and 106.62%, but average speed decreased about 42.35%. Moreover, In case of a day after earthquake, LOS changed to C level (up 1 level), where traffic volume, VKT, VHT, and average speed decreased approximately 23.35%, 24.93%, 6.43%, and 19.77%, respectively.

5. Conclusions

The development of travel demand models under earthquake using spaghetti and meatballs method and four-step transportation model can use to evaluate the vulnerability of both road network and area-covering disruptions, and forecast travel demand, travel behavior, travel pattern, and traffic volume, respectively. Moreover, the resulting model can provide government and related agencies profound information in planning and developing either pre- or post-disaster operations. However, when the developed models applied to the simulated geographical area with simulated road network found that the traffic conditions before and after the earthquake were different. The traffic condition after the earthquake is worse than before the earthquake. In case of an hour after earthquake, level of service (LOS) changed from B to D level (up 2 levels) and changed to C level (up 1 level) in case of a day after earthquake.

6. Acknowledgment

This research work was partially supported by Chiang Mai University, Thailand.

7. References

- [1] A. J. Pel, M. C. J. Bliemer, and S. P. Hoogendoorn. "A review on travel behaviour modelling in dynamic traffic simulation models for evacuations". *Transportation*, vol. 39, pp. 97-123, January 01, 2012.
- [2] S. Andrews, H. Wang, D. Ni, S. Gao, and J. Collura. "Development and implementation of an adapted evacuation planning methodology in the framework of emergency management and disaster response: A case study using TransCAD". *Journal of Transportation Safety and Security*, vol. 2, pp. 352-368, 2010.
- [3] C. C. Yang, B. R. Tsai, and C. C. Ho. "The application of systems thinking for problem solving of self-precaution community against flood". *Taiwan Water Conservancy*, vol. 64, pp. 55-61, 2016.
- [4] L. Yang, H. Tatano, Y. Kajitani, and X. Jiang. "A case study on estimation of business interruption losses to industrial sectors due to flood disasters". *Journal of Disaster Research*, vol. 10, pp. 981-990, 2015.
- [5] Y. Y. Hsiao, C. F. Chen, S. H. Chiang, and N. T. Son. "Change detection of rice fields after the Great East Japan Tsunami using time-series MODIS data". 2014.
- [6] F. E. Kung, H. Y. Hu, J. F. Jan, Y. C. Shao, M. Y. Li, K. S. Yeh, *et al.*. "Object-oriented classification for extracting landslides from DMC aerial images". 2013, pp. 1254-1262.
- [7] M. Xiang, W. Zhao, and J. Chen. "A comparison of different reconstruction modes and adaptive evaluation systems for community recovery following the Wenchuan Earthquake". *Sustainability (Switzerland)*, vol. 10, 2018.
- [8] Q. Li, J. Zhang, L. Gong, T. Xue, and H. Jiang. "Extraction of earthquake-collapsed buildings based on correlation change detection of multi-texture features in SAR images". *Yaogan Xuebao/Journal of Remote Sensing*, vol. 22, pp. 128-138, 2018.
- [9] L. Wang, A. Dou, X. Wang, Y. Dong, X. Ding, Z. Li, *et al.*. "Damage assessment of Haiti earthquake emergency using high resolution remote sensing imagery". 2011.
- [10] B. Saeidian, M. S. Mesgari, B. Pradhan, and M. Ghodousi. "Optimized Location-Allocation of Earthquake Relief Centers Using PSO and ACO, Complemented by GIS, Clustering, and TOPSIS". *ISPRS International Journal of Geo-Information*, vol. 7, pp. 292, 2018.
- [11] N.Y. Yun, and M. Hamada. "Evacuation behavior and fatality rate during the 2011 Tohoku-Oki earthquake and tsunami". *Earthquake Spectra*, vol 31(3), pp. 1237-1265, 2015.
- [12] R. Heath. "The Kobe earthquake: Some realities of strategic management of crises and disasters". *Disaster Prevention and Management: An International Journal*, vol. 4(5), pp. 11-24, 1995.
- [13] G. Chiaro, G. Alexander, P. Brabhakaran, C. Massey, J. Koseki, S. Yamada, *et al.*. "Reconnaissance report on geotechnical and geological aspects of the 14-16 April 2016". *Kumamoto earthquakes*, Japan. 2017.
- [14] N. Mimura, K. Yasuhara, S. Kawagoe, H. Yokoki, S. Kazama. "Damage from the Great East Japan Earthquake and Tsunami-a quick report". *Mitigation and adaptation strategies for global change*, vol. 16(7), pp. 803-818, 2011.
- [15] T. Yaba, S. Ikemoto. "Cross-comparative analysis of evacuation behavior after earthquakes using mobile phone data". *PLoS One*, vol 14(2), 2019.
- [16] A. Soltani, A. Ardalan, A. Darvishi Bolorani, A. Haghdoost, and M. J. Hosseinzadeh-Attar. "Site selection criteria for sheltering after earthquakes: a systematic review". *PLoS Curr*, vol. 6, Aug 29 2014.

-
- [17] D. Contreras, T. Blaschke, S. Kienberger, and P. Zeil. "Spatial vulnerability indicators: "Measuring" recovery processes after earthquakes". 2011.
- [18] V. Maliene, V. Grigonis, V. Palevičius, and S. Griffiths. "Geographic information system: Old principles with new capabilities". *URBAN DESIGN International*, vol. 16, pp. 1-6, 2011/01/01 2011.
- [19] J. Pence, I. Miller, T. Sakurahara, J. Whitacre, S. Reihani, E. Kee, *et al.*. "GIS-Based Integration of Social Vulnerability and Level 3 Probabilistic Risk Assessment to Advance Emergency Preparedness, Planning, and Response for Severe Nuclear Power Plant Accidents". *Risk Analysis*, vol. 39, pp. 1262-1280, 2019.
- [20] L. K. R. Putri and M. Maryono. "Assessing Evacuation Route Against Mount Merapi Hazard by Using Least Cost Path Method in Mriyan-Boyolali, Indonesia". 2018.
- [21] J. Jiang, P. Wang, W. S. Lung, L. Guo, and M. Li. "A GIS-based generic real-time risk assessment framework and decision tools for chemical spills in the river basin". *Journal of Hazardous Materials*, vol. 227-228, pp. 280-291, 2012.
- [22] A. Trozzi, M. De Amicis, M. Deligios, S. Frigerio, S. Sironi, and S. Sterlacchini. "GIS and Decision Support System techniques for the emergency management in at-risk industrial areas". *Rendiconti Online Societa Geologica Italiana*, vol. 8, pp. 155-158, 2009.
- [23] A. Agrawal, S. S. Udmale, and V. K. Sambhe. "Extended Four-Step Travel Demand Forecasting Model for Urban Planning". *Information and Communication Technology for Sustainable Development*, Singapore, pp. 191-198, 2018.
- [24] J. Zhang, X. Feng, and A. Fujiwara. "Comprehensive Travel Demand Analysis in Asian Developing Megacities". in *Sustainable Transport Studies in Asia*, A. Fujiwara and J. Zhang, Eds., ed Tokyo: Springer Japan, pp. 65-86, 2013.
- [25] R. Mustafa and M. Zhong. "Challenges and opportunities in applying high-fidelity travel demand model for improved network-wide traffic estimation: A review and discussion". *Open Transportation Journal*, vol. 8, pp. 1-18, 2014.
- [26] Dougenik, and A. James. "WHIRLPOOL: A geometric processor for polygon coverage data". *Proc. AUTO-CARTO*, vol. 4, pp. 304-311, 1979.
- [27] D. J. Peuquet, and D. F. Marble. *"Introductory readings in Geographic Information Systems"*. London-New York-Philadelphia: Taylor & Francis, 1990.
- [28] United States Department of the Interior, Washing, D.C. Geological Survey. *Earthquake Information Bulletin*. vol. 13(14), 1981.
- [29] J.D. Ortúzar, and L.G. Willumsen. *"Modeling Transport"*. New York: John Wiley & Sons, 1990.
- [30] V.H. Brustlin, *"Transportation Demand Management Plan"*. Verginia: University of Verginia, 2007.
- [31] M. Steinhoff, and J. Harpring. *"Transportation and Sustainability on the Indiana University"*. Bloomington: Bloomington Campus, Indiana University, 2008.
- [32] Comsis Corporation. *"UTPS Highway Network Development Guide"*, Federal Highway Administration, US Department of Transportation, 1983.
- [33] A. A. Amavia, J. P. Romerob, A. Domingueza, L. Olioia, A. Ibeas. "Advanced trip generation/attraction models". *Procedia - Social and Behavioral Sciences*, vol. 160 pp. 430 – 439, 2014.
- [34] D. McFadden. *"Economic Choices"*. American Economic Review, vol. 91, pp. 351-378, 2001.
- [35] L. Zhu, and J. Cao. *"A Network Equilibrium Model for Emergency Logistics Response under Disaster Spreading"*. 2010 International Conference on Logistics Engineering and Intelligent Transportation Systems (LEITS), pp. 1-4, 2010.

Piano Keyboard 3D Pedestrian Crossing Evaluation: The case of Chiang Mai University Demonstration School

**Preda Pichayapan^{ab}, Thanatchaporn Peansara^{ab},
Patcharapan Nanthavisit^{ab}, Jessada Pochan^c**

^aDepartment of Civil Engineering, Faculty of Engineering, Chiang Mai University, Thailand

^bExcellence Center in Infrastructure Technology and Transportation Engineering, Chiang Mai University

^cFaculty of Industrial Technology, Pibulsongkram Rajabhat University, Thailand

Email Address: markpochan@gmail.com

Abstract

Traffic accidents involving pedestrians become a main problem in Thailand. Fatalities and serious injuries are often happened when an accident occurs at pedestrian crossing. In 2018, World Health Organization reported that 7.6% of injured accidents in Thailand involved pedestrians. By using 3D pedestrian crossing, it is expected that accident situation might be improved. The 3D pedestrian crossing is designed as in a piano keyboard shape using perspective technique, and installed Chiang Mai University Demonstration School. Then, this research evaluates speeds of vehicles before and after installed the 3D pedestrian crossing. After installation of the 3D Pedestrian crossings, visual inspections of the crossings are conducted for three months, day and night. It is found that visualization of the 3D image is deteriorated over time. Using the 3D pedestrian crossings, the vehicle speed is reduced. However, the speed reduction is continued only for the first 3 weeks. Therefore, 3D crossing might be appropriate for short-term speed reduction.

Keywords: 3D Pedestrian Crossing, Pedestrian Crossing Evaluation, Speed Calming

- *This research presented on 42th International Conference on Engineering, Technology and Applied Science (ETAS-42): Tokyo/Japan, January, 14th, 2020*

1. Introduction

The excessive speed is a common cause of accident [1], some country adopted 3D image to apply in crossing in order to slow traffic, such as New Delhi, China, Iceland, South Africa, Britain, US, Russia, Ukraine, Kyrgyzstan, New Zealand and Greece. The 3D crossing is a modern system that affect to geometric design, the purpose of 3D crossing is to be conspicuous, to increase drivers' awareness and the drivers to slow down. Because 3D-paint gives the optical illusion of the white stripes floating above the ground and obstructing the road [2].

Rebelo, F. et al. studied the driver reaction for 2D and 3D crosswalks. Results seems to show that people take longer to respond to the 3D crosswalk but make more mistakes on the 2D crosswalk [3]. Moreover, the shape of 3D crosswalks effect to the drivers' willingness to reduce vehicle speed, Trifunović, A. et al. studied the two types of road markings: the square shape base (rectangular prism) and the triangular shape base (triangular prism). The drivers' willingness to reduce vehicle speed more response to the square shape base [4].

In Thailand and Southeast Asia, pedestrian traffic accidents become a major problem. Fatalities and serious injuries are often happened, when an accident occurring at pedestrian crossing. In 2018, World Health Organization reported that Thailand has injury accidents at the pedestrian of 7.6% [1]. A higher pedestrian traffic accidents rate, using 3D crossing is the decent choice to reduce speed and decrease pedestrian traffic accidents rate. Uttaradit province and Phitsanulok province have brought 3D crossing as rectangular prism to reduce speed of vehicles. However, there are no evaluations for 3D crossing in Thailand.

In the past researches [3, 4], the 3D crossing affects speed reduction and driver's behaviors. The vehicle speeds are reduced when installed rectangular prism 3D crossing. A more conspicuous shape is expected to be applied for the 3D crossing. Therefore, piano keyboard shape is used in this study. A piano keyboard 3D pedestrian crossing is installed on a road in Chiang Mai University Demonstration School area. Then, the 3D crossing is evaluated by comparing the vehicle speeds before and after installation of the crossing. Data is gathered by visualization of the 3D image for 3 months.

2. Methodology

The experiment was performed to explore speed of vehicles at 3D crossing. The 3D pedestrian crossing was painted instead of the exiting 2-D crossing on the road in Chiang Mai University Demonstration School area. It was designed as a piano keyboard shape by perspective technique. Then, this research studies before and after installed the 3D pedestrian crossing. This research studies two types of vehicle; motorcycle and personal car.

The exiting pedestrian crossing or 2D crossing speed was surveyed for comparing with the new 3D pedestrian crossing. This research observed average speed and 85th percentile speed of vehicles (150 vehicles of motorcycle and 150 vehicles of personal car) by using a video camera.

The speeds were observed at different points in time - before painting, 1 day, 1 weeks, 2 weeks, 3 weeks, 4 weeks, 8 weeks and 12 weeks after painting. Moreover, the quality of 3D crossing was observed during daytime and night time for 12 weeks as well.

3. 2-D Image Pedestrian Crossing (Exiting Crossing)

The exiting pedestrian crossing or 2D crossing is shown in Figure 1 as a zebra pedestrian crossing. It was installed on the two lanes road in front of Chiang Mai University Demonstration School, with shoulder of 7.43-meter width.

Average speed of vehicles on this road before the painting 3D crossing is 35.25 kph for motorcycles and 34.32 kph for personal cars. The 85th percentile speed of motorcycles and personal cars are 40.45 kph and 34.32 kph, respectively. These speeds are higher than the school zone speed limit (30 kph.) [5].



Figure 1: The exiting pedestrian crossing or 2D crossing

4. Piano Keyboard 3D Image Pedestrian Crossing Design

The piano keyboard shape is like a zebra pedestrian crossing but piano image is more conspicuous than as a zebra pedestrian crossing. This 3D image pedestrian crossing was designed by perspective technique at horizon line 1.19 m. height [6]. The vanishing point that can be seen the 3D crossing at 20 m. before stopping line according to breaking distance for vehicle speed 40 kph.

The speed 30 kph is speed limit for school zone. The breaking distance is 10.3 m. (10 m.) but the speed of vehicles in this area is 34-43 kph. Then, the speed 40 kph will be selected to design speed and to calculate breaking distance. The breaking distance of speed 40 kph is 18.4 m. (20m.). This distance was designed the vanishing point of piano keyboard 3D image pedestrian crossing (Figure 2.).

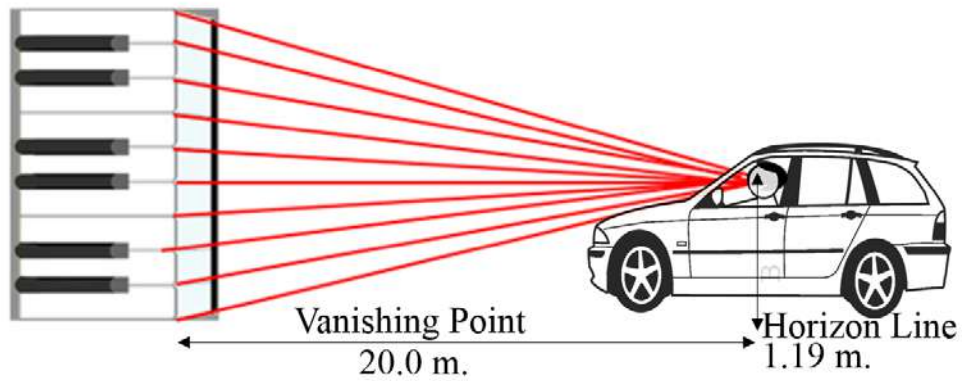


Figure 2: The vanishing point and the horizon line

The 3D pedestrian crossing was designed to be seen at 20 m. by adapting Manual of Application for Traffic Control Devices at crossing in Urban Community and Schools Area. [7] The dimensions of piano 3D image pedestrian crossing are shown in Figure 3. The white strip of crossing widens 0.80 m. and a length of 4.00 m. The black strip is 0.37 m. width with a length of 2.80 m.

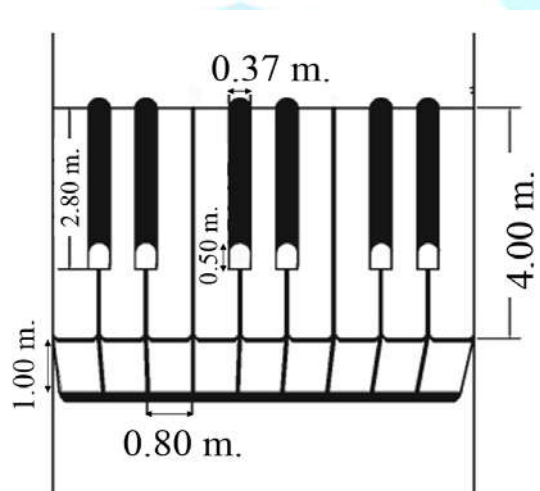


Figure 3: Piano keyboard 3D image crossing dimension

The height of the piano keyboard (white strips) is 1.00 m. in order to be designed by sketch from horizon line to vanishing point. The black strip's height is 0.50 m.

The 3D painted use the thermoplastic color. This materials for road marking were supported by 3M Thailand Co., Ltd., TOA PAINT Thailand Co., Ltd. and The Siam Cement Group Public Company Limited. The new pedestrian crossing was installed as shown in Figure 4.



Figure 4: Piano 3D image crossing located on Chiang Mai University Demonstration School

5. Result and Discussion

5.1 Speed of vehicle before arriving 3D image crossing

5.1.1 Speed of Motorcycles at 3D image crossing

The speeds of motorcycles are shown in Table 1. The results show average speeds and the 85th percentile speed at 3D image crossing both before and after 3D crossing installation.

Before installing the 3D crossing, the 85th percentile speed of motorcycles at 3D image crossing is 40.45 kph while, the average speed is 35.21 kph. One day after the installation, not only the average speed, but also the 85th percentile speed decreases approximately 6%. The lowest average speed is found at 2 weeks after the installation, where the speeds rise to almost the same speed as before 3D crossing being painted. After week 12, the speed is higher than the speed before painting as shown in Figure 5.

Comparison of mean test is performed to compare average speed of motorcycles before and after installing 3D crossing, with a significance level of 0.05. The comparison results, shown in Table 1, show that average speeds at 1 Day, 1 week, 2 weeks and 3 weeks after installing are different from speeds before 3D installation. However, the average speeds after 4 weeks, 8 weeks and 12 weeks are indifferent. Thus, the speed reduction is only contained for the first 3 weeks.

Table 1: The 85th percentile speed and average speed of motorcycles at the 3D crossing

Date observed	The 85 th percentile speed (kph)	Average speed (kph)	S.D.	Z	Sig. 0.05
before painting	40.45	35.21	5.75	-	-
1 day	37.85	30.66	6.14	6.606	.000
1 week	37.51	31.29	6.32	5.596	.000
2 weeks	36.03	30.00	6.00	7.654	.000
3 weeks	38.55	32.04	5.22	4.977	.000
4 weeks	40.32	35.21	5.85	1.224	.086
8 weeks	43.41	34.53	8.09	0.825	.429
12 weeks	44.55	35.42	8.03	-0.259	.778

5.1.2 Speed of personal cars at 3D image crossing

The speeds of personal cars at a crossing are presented in Table 2. The speeds are of similar trend of motorcycles' speed. The results have shown average speeds and the 85th percentile speed at 3D image crossing both before and after the 3D crossing installation.

Before installing the 3D crossing, the 85th percentile speed of personal cars at 3D image crossing is 38.30 kph while, the average speed is 34.32 kph. One day after the installation, not only the average speed, but also the 85th percentile speed decreases approximately 4%. The speeds fluctuate until 4 weeks later, and then rise up to almost same speed as before painting 3D crossing. At 12th week, the speed is higher than the speed before painting as shown in Figure 5.

Comparison of mean test is performed to compare average speed of personal cars before and after installing 3D crossing with a significance level of 0.05. The comparison results, shown in Table 2, show that average speeds at 1 day, 1 week, 2 weeks and 3 weeks after installing are different from speeds before 3D installation. However, the average speeds after 4 weeks, 8 weeks and 12 weeks are not different. Thus, the speed reduction is contained for the 3 weeks after installing.

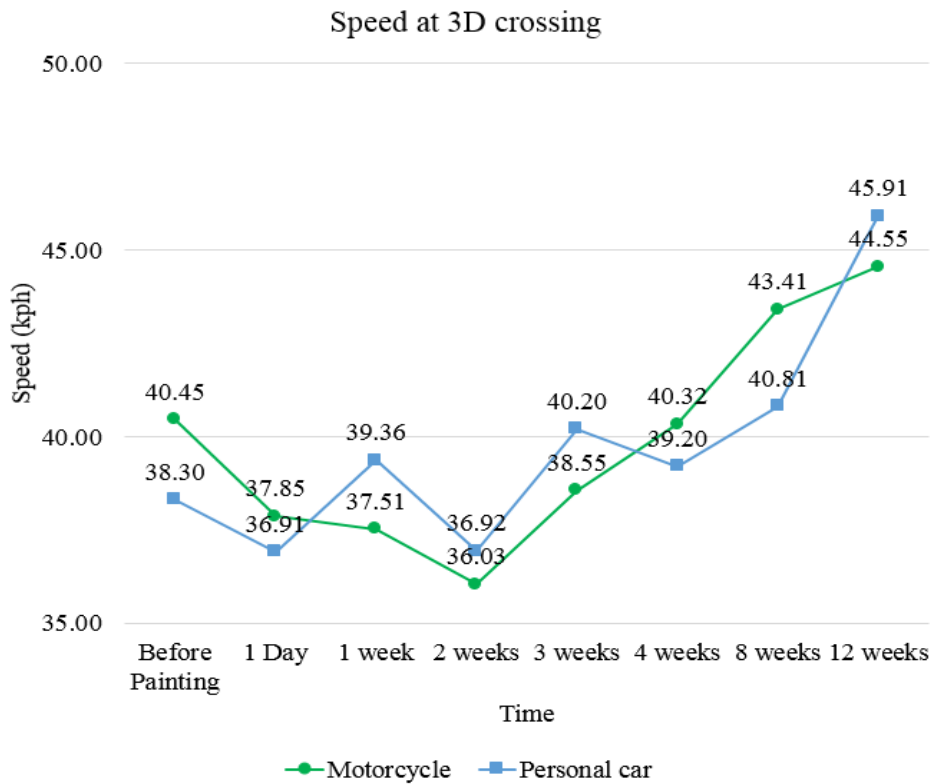


Figure 5: The average speeds of motorcycles and personal cars at the 3D crossing

Table 2: The 85th percentile speed and average speed of personal cars at the 3D crossing

Date observed	The 85 th percentile speed (kph)	Average speed (kph)	SD	Z	Sig. 0.05
before painting	38.30	34.32	5.75	-	-
1 day	36.91	30.66	6.14	6.027	.000
1 week	39.36	31.29	6.32	4.882	.000
2 weeks	36.92	30.32	6.00	5.940	.000
3 weeks	40.20	32.64	5.22	2.406	.008
4 weeks	39.20	33.58	5.85	1.402	.080
8 weeks	40.81	33.58	8.09	0.286	.387
12 weeks	45.91	34.68	8.03	-0.422	.336

5.1.3 The quality of 3D image crossing

Piano keyboard 3D crossing in daytime after installing 1 week is shown in Figure 6. The crossing can be clearly seen in daytime. After installing 12 weeks, the 3D crossing was covered with dirt as depicted in Figure 7.



Figure 6: Piano keyboard 3D crossing in daytime after installing 1 week



Figure 7: Piano keyboard 3D crossing in daytime after installing 12 weeks

The 3D crossing in night-time after installing 1 week is presented in Figure 8. The light from vehicle reflects on the crossing then 3D crossing can be clearly seen in night-time. After installing 12 weeks, the 3D crossing almost cannot be seen in night-time as shown in Figure 9.

After installation of the 3D Pedestrian crossings, visual inspections for the crossings are carried out for both daytime and night time. It is found that visualization of the 3D image is deteriorated over time. As a result, routine maintenance, surface cleaning, for the 3D pedestrian crossing is recommended.



Figure 8: Piano keyboard 3D crossing in night-time after installing 1 week



Figure 9: Piano keyboard 3D crossing at night after having installed for 12 weeks

6. Conclusion

The 3D Pedestrian crossing was designed as piano keyboard by using perspective technique to be more conspicuous. After installed 3D crossing, the average speed and the 85th percentile speed were observed. The average speed and the 85th percentile speed immediately reduced. However, the speed reduction is contained for the first 3 weeks, and then the speeds rise up as close to the speed before painting 3D crossing.

Moreover, comparison of mean test is performed which indicates average speed of vehicles before and after installing 3D crossing, testing with the significance level of 0.05. The average speeds after 1 day until 3 weeks of installation are different. It means that the 3D crossing effect on the speed reduction remains for 3 weeks only. It is possibly because the drivers have become familiar with the 3D crossing. However, 3D crossing might still be appropriate for short-term speed reduction.

In the beginning, the crossing can be conspicuous in daytime and night time, while after 3 months, routine maintenance and surface cleaning for the 3D pedestrian crossing are required as of visualization of the 3D image is deteriorated over time.

7. Acknowledgment

This research work was partially supported by Chiang Mai University and Pibulsongkram Rajabhat University, Thailand. The authors gratefully acknowledge the installing staffs from the Department of Rural Road, the materials for road marking from 3M Thailand Co., Ltd., TOA PAINT Thailand Co., Ltd. and The Siam Cement Group Public Company Limited, and the installation site from Chiang Mai University Demonstration School, Faculty of Education, Chiang Mai University.

8. References

- [1] World health organization. Global status report on road safety. (2018).
- [2] Hasson, P., Struve, B., Chen, C., Brewer, J., Doctor, M., Harrison, K., Maifield, D., Matzke, M., Merritt, G., & Mooney, R.. Evolving Geometric Design Decision-Making in the United States. U.S. Country Report for the 5th International Symposium on Geometric Design. Vancouver, Canada. (2015).
- [3] Rebelo, F., Cerqueira, D., Freixinho, I., and Noriega, P. Evaluation of 3D crosswalks design. *Advances in Intelligent Systems and Computing*, Volume 777, 89-96. (2019).
- [4] Trifunović, A. V., Čicević, S. J., Lazarević, D. M., Dragović, M. S., Vidović, N. D., Mošić, M. R., and Otat, O. V. Perception of 3D virtual road markings - based on estimation of vehicle speed. *FME Transactions*, 47(2), 360-369. (2019).
- [5] Department of Rural Road. Standard of Drawing. (2016). (in Thai)
- [6] Pedpradab P. and Rudjanakanoknad J., Eye Height and Reaction Time for Thai Drivers. 19th National Convention on Civil Engineering, 14-16 May 2014, Khon Kaen, THAILAND. (2014). (in Thai)
- [7] Department of Highways. Manual of Application for Traffic control Devices at crossing in Urban Community and Schools Area, THAILAND. (2011). (in Thai)



AASE INTERNATIONAL CONFERENCE

AASE International Conference serves as platform that aims to provide opportunity to the academicians and scholars from across various disciplines to discuss interdisciplinary innovations. It's so happy to see the papers from all part of the world published in this proceedings. This proceeding brings out the various Research papers from diverse areas of science, engineering, technology, management, business and education. These articles that received for these conferences are very promising and impactful. We believe these studies have the potential to address key challenges in various sub domains of social sciences and applied sciences.

